

Contrasting fluids and reservoirs in the contiguous Marcona and Mina Justa iron oxide–Cu (–Ag–Au) deposits, south-central Perú

Huayong Chen · T. Kurtis Kyser · Alan H. Clark

Received: 12 January 2010 / Accepted: 3 March 2011 / Published online: 24 March 2011
© Springer-Verlag 2011

Abstract The Marcona–Mina Justa deposit cluster, hosted by Lower Paleozoic metaclastic rocks and Middle Jurassic shallow marine andesites, incorporates the most important known magnetite mineralization in the Andes at Marcona (1.9 Gt at 55.4% Fe and 0.12% Cu) and one of the few major iron oxide–copper–gold (IOCG) deposits with economic Cu grades (346.6 Mt at 0.71% Cu, 3.8 g/t Ag and 0.03 g/t Au) at Mina Justa. The Middle Jurassic Marcona deposit is centred in Ica Department, Perú, and the Lower Cretaceous Mina Justa Cu (Ag, Au) prospect is located 3–4 km to the northeast. New fluid inclusion studies, including laser ablation time-of-flight inductively coupled plasma mass spectrometry (LA-TOF-ICPMS) analysis, integrated with sulphur, oxygen, hydrogen and carbon isotope analyses of minerals with well-defined paragenetic relationships, clarify the nature and origin of the hydrothermal fluid responsible for these contiguous but genetically contrasted deposits. At Marcona, early, sulphide-free stage M-III magnetite–biotite–calcic amphibole assemblages are inferred to have crystallized from a 700–800°C Fe oxide melt with a $\delta^{18}\text{O}$ value from +5.2‰ to

+7.7‰. Stage M-IV magnetite–phlogopite–calcic amphibole–sulphide assemblages were subsequently precipitated from 430–600°C aqueous fluids with dominantly magmatic isotopic compositions ($\delta^{34}\text{S}=+0.8‰$ to +5.9‰; $\delta^{18}\text{O}=+9.6‰$ to +12.2‰; $\delta\text{D}=-73‰$ to $-43‰$; and $\delta^{13}\text{C}=-3.3‰$). Stages M-III and M-IV account for over 95% of the magnetite mineralization at Marcona. Subsequent non-economic, lower temperature sulphide–calcite–amphibole assemblages (stage M-V) were deposited from fluids with similar $\delta^{34}\text{S}$ (+1.8‰ to +5.0‰), $\delta^{18}\text{O}$ (+10.1‰ to +12.5‰) and $\delta^{13}\text{C}$ (–3.4‰), but higher δD values (average $-8‰$). Several groups of lower (<200°C, with a mode at 120°C) and higher temperature (>200°C) fluids can be recognized in the main polymetallic (Cu, Zn, Pb) sulphide stage M-V and may record the involvement of modified seawater. At Mina Justa, early magnetite–pyrite assemblages precipitated from a magmatic fluid ($\delta^{34}\text{S}=+0.8‰$ to +3.9‰; $\delta^{18}\text{O}=+9.5‰$ to +11.5‰) at 540–600°C, whereas ensuing chalcocite–bornite–digenite–chalcocite–hematite–calcite mineralization was the product of non-magmatic, probably evaporite-sourced, brines with $\delta^{34}\text{S}\geq+29‰$, $\delta^{18}\text{O}=0.1‰$ and $\delta^{13}\text{C}=-8.3‰$. Two groups of fluids were involved in the Cu mineralization stage: (1) Ca-rich, low-temperature (approx. 140°C) and high-salinity, plausibly a basinal brine and (2) Na (–K)-dominant with a low-temperature (approx. 140°C) and low-salinity probably meteoric water. LA-TOF-ICPMS analyses show that fluids at the magnetite–pyrite stage were Cu-barren, but that those associated with external fluids in later stages were enriched in Cu and Zn, suggesting such fluids could have been critical for the economic Cu mineralization in Andean IOCG deposits.

Editorial handling: R.P. Xavier

H. Chen (✉) · T. K. Kyser · A. H. Clark
Department of Geological Sciences & Geological Engineering,
Queen's University,
Kingston, ON, Canada K7L 3N6
e-mail: huayong.chen@utas.edu.au

Present Address:

H. Chen
ARC Centre of Excellence in Ore Deposit Research (CODES),
University of Tasmania,
Private Bag 126,
Hobart, Tasmania 7001, Australia

Keywords Fluid sources and evolution · Fluid inclusions · Stable isotopes · IOCG deposits · Central Andes · Peru

Introduction

Iron oxide–copper–gold (IOCG) deposits have become a major exploration and research target in the last 30 years, prompting extensive discussion of their salient geological features. The extraordinary range of IOCG deposits and resulting controversy regarding the nature, sources and interrelationships of the ore-forming fluids has impeded ore-genetic modelling, although several classifications have been proposed (Williams 2010; Groves et al. 2010). Characterization of IOCG mineralizing fluids has included conventional microthermometric analysis of fluid inclusions in several major deposits, including Olympic Dam (Oreskes and Einaudi 1992) and Ernest Henry (Mark et al. 2000) in Australia and La Candelaria in Chile (Ullrich and Clark 1999), but more sophisticated analytical techniques have been applied only to a few examples. Thus, proton-induced X-ray emission analyses of individual fluid inclusions have been documented for the Starra (Williams et al. 2001) and magnetite-dominant Lightning Creek (Perring et al. 2000) deposits in Australia and for the Wernecke Breccia in Canada (Gillen et al. 2004), and laser Raman spectroscopic methods have been applied at Starra (Williams et al. 2001) and probably IOCG-like Pahtohavare, Sweden (Lindblom et al. 1996) and Bidjovagge, Norway (Ettner et al. 1994). On the basis of this limited database, some researchers interpret IOCG deposits as magmatic–hydrothermal systems involving moderate-temperature (~300–450°C), high-salinity and CO₂-rich ore-forming fluids (e.g. Xu and Pollard 1999; Pollard 2000, 2001, 2006; Fu et al. 2003). Such fluids have been identified at Eloise (Baker 1998), La Candelaria (Ullrich and Clark 1999) and Ernest Henry (Mark et al. 2000), in all cases directly associated with chalcopyrite–gold mineralization; moderate-temperature fluid inclusions were also trapped in the pre-mineralization “ironstone” stage at Starra (Williams et al. 2001) and Lightning Creek (Perring et al. 2000). Nevertheless, many IOCG deposits, particularly at their Cu–Au mineralization stages, are characterized by medium to lower temperature (<300°C), high-salinity, Ca-rich fluids with variable CO₂ contents, ascribed to non-magmatic reservoirs, as at Olympic Dam (Oreskes and Einaudi 1992), Pahtohavare (Lindblom et al. 1996) and Wernecke (Gillen et al. 2004; Hunt et al. 2005, 2007). Furthermore, multisource mixing models, involving fluids with variable temperatures, salinities and chemical compositions, have been proposed by Haynes et al. (1995), Williams et al. (2001, 2005), Barton and Johnson (2004) and Hunt et al. (2005, 2007) for the Cu–Au stage of IOCG deposits.

Stable isotope geochemistry has been used to identify the dominant fluid source in IOCG deposits, including those of the Olympic Dam district (Oreskes and Einaudi 1992; Bastrakov et al. 2007), Raúl-Condestable (Ripley and Ohmoto 1977; de Haller et al. 2002, 2006), Bidjovagge

(Ettner et al. 1994), Starra (Rotherham et al. 1998; Williams et al. 2001), La Candelaria (Ullrich and Clark 1999; Ullrich et al. 2001; Marschik and Fontboté 2001), Lightning Creek (Perring et al. 2000), Ernest Henry (Mark et al. 2000; Mark and Oliver 2006), Eloise (Baker et al. 2001) and Mantoverde (Benavides et al. 2007). However, the major sources of sulphur and/or associated metals remain uncertain in many examples (Williams et al. 2005) and, as with fluid inclusion studies, interpretations of the source of the mineralizing fluids advocate two contrasting models: a dominance of either magmatic–hydrothermal (Pollard 2000, 2001, 2006) or external, non-magmatic fluids (Barton and Johnson 1996, 2000, 2004) as key contribution to mineralization. Thus, at Ernest Henry (Mark et al. 2000; Mark and Oliver 2006) and Eloise (Baker et al. 2001), most calculated $\delta^{34}\text{S}_{\text{fluid}}$ values are magmatic (~0‰), whereas at La Candelaria (Ullrich and Clark 1999; Ullrich et al. 2001; but cf. Marschik and Fontboté 2001), Raúl-Condestable (de Haller et al. 2006) and Mantoverde (Benavides et al. 2007), the calculated $\delta^{34}\text{S}_{\text{fluid}}$ values for Cu–Au mineralization are much higher, which predicate external fluid involvement. In addition, ore-forming fluids through mid-crustal fluid mixing or metamorphism have been documented at Ernest Henry (Kendrick et al. 2007) and Osborne (Fisher and Kendrick 2008).

The major controversy on the genesis of IOCG deposits therefore focuses on the nature and source of fluids responsible for Cu–Au mineralization and their relationship to those at the precursor magnetite stage. The Marcona–Mina Justa deposit cluster in south-central Perú, incorporating the largest concentration of magnetite and one of the major IOCG-type Cu deposits in the Central Andes, provides an excellent context for comparison of the ore-forming fluids in the Andean IOCG systems with and without economic Cu mineralization (Fig. 1). The Marcona iron mine has present reserves of 1,551 Mt grading 55.4% Fe and 0.12% Cu, and annual production in recent years has averaged 4–5 Mt of magnetite concentrates (Shougang Hierro Perú SA., Resource Estimate of the Marcona Iron Mine, unpublished report, 2003, in Chinese). The Mina Justa Cu (Ag–Au) deposit, under development by Chariot Resources and with 346.6 Mt at an average grade of 0.71% Cu, 3.83 g/t Ag and 0.03 g/t Au, at a cutoff grade of 0.2% Cu (Mining Journal, Nov. 24, 2006, p. 8), is located 3–4 km northeast of the Marcona mine. The detailed geology of the Marcona–Mina Justa district and its deposits, including paragenetic relationships, geochronology and geothermometric constrains, has been documented in Chen et al. (2010a, 2010b). Herein, we present microthermometric data for fluid inclusions in hydrothermal calcite from Marcona and in quartz and calcite from Mina Justa, as well as compositions of quartz-hosted inclusions obtained by laser ablation time-of-flight inductively coupled plasma mass

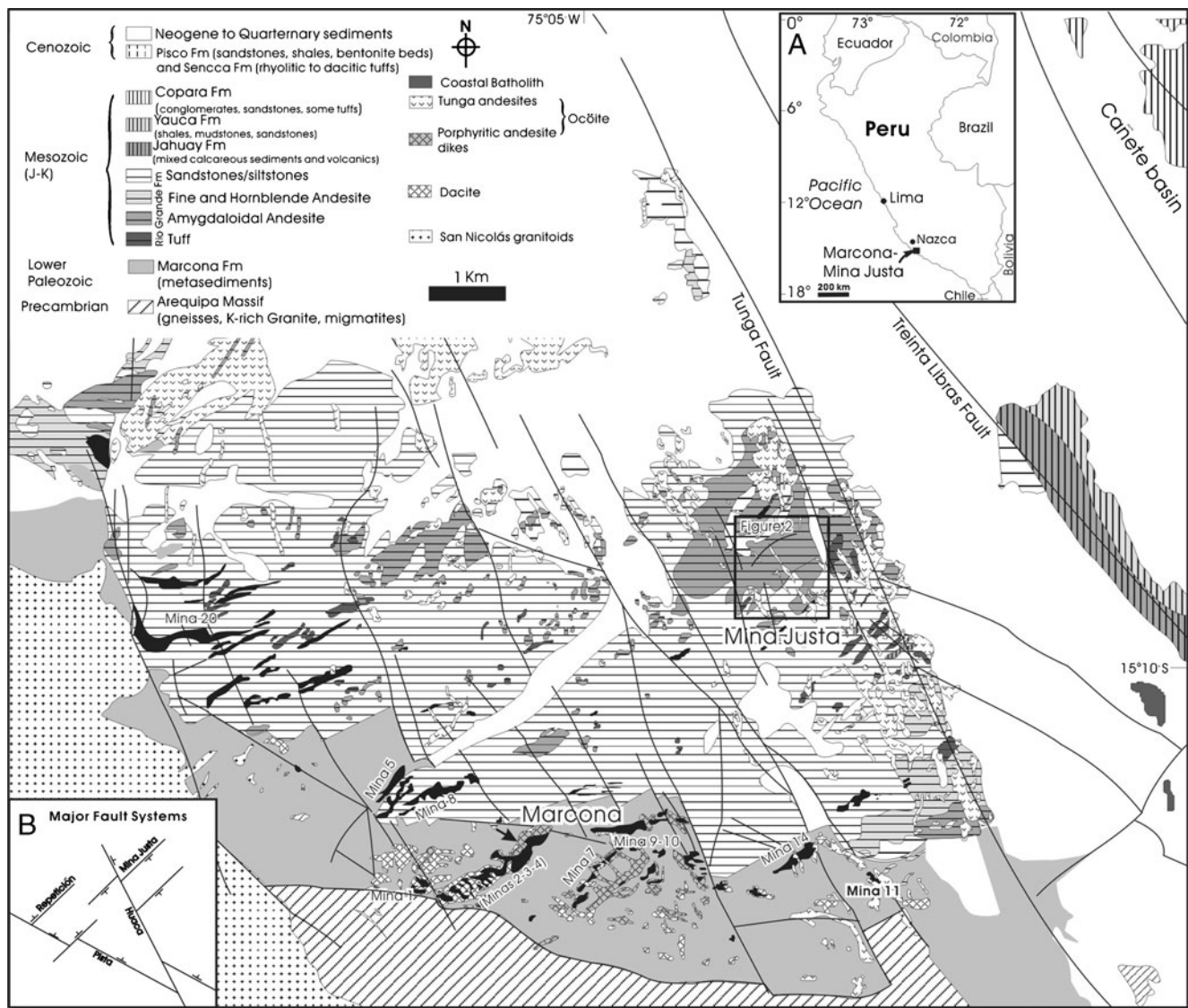


Fig. 1 Geology of the area surrounding the Marcona and Mina Justa deposits (modified from Rio Tinto, Marcona JV exploration report, June 2003). *Insert A* shows the location of the study area and *B* the local major fault systems

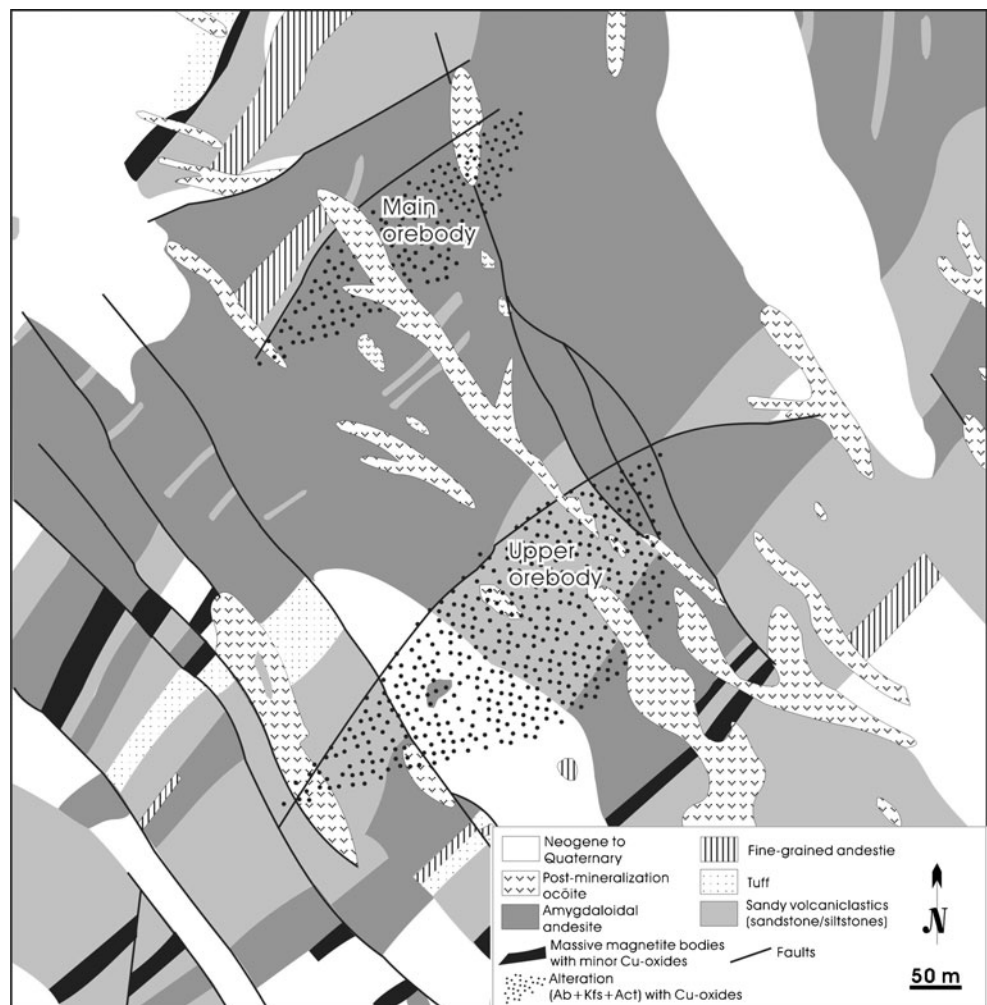
spectrometry (LA-TOF-ICPMS) analysis. These data are integrated with stable sulphur, oxygen, hydrogen and carbon isotope analyses to define the relative contributions of various fluid reservoirs to the magnetite- and sulphide-dominant assemblages of the two deposits.

District and deposit geology

The Marcona–Mina Justa district is underlain by metamorphic rocks of the Proterozoic Arequipa Massif, covered by Neoproterozoic and Paleozoic sedimentary strata and, more extensively, by Mesozoic volcanic and sedimentary rocks which accumulated in a succession of intra- and back-arc

rift basins (Fig. 1; Atherton and Webb 1989; Hawkes et al. 2002). Granitoid rocks of the Lower Palaeozoic (425± 4 Ma: Mukasa and Henry 1990; Vidal et al. 1990) San Nicolás Batholith intruded the Lower Palaeozoic metasedimentary Marcona Formation that hosts much of the Marcona magnetite mineralization and which comprises thermally metamorphosed siltstone, sandstone, minor quartz arenite and limestone. The overlying Mesozoic volcano-sedimentary sequence was intruded by the Late Aptian (112–120 Ma: de Haller et al. 2006) Coastal Batholith. In contrast, all Cu (Ag–Au) mineralization at Mina Justa is hosted by the Middle Jurassic Río Grande Formation (Figs. 1 and 2), which is dominated by plagioclase-phyric andesite and andesitic volcanoclastic

Fig. 2 Geological map of the Mina Justa Cu deposit, hosted by the Middle Jurassic Upper Río Grande Formation (modified from Rio Tinto 1: 10,000 mapping of Mina Justa deposit, February 2003, unpublished report). *Ab* albite, *Kfs* K-feldspar, *Act* actinolite



units with minor sandstone, siltstone and limestone lenses (Caldas 1978; Hawkes et al. 2002; Baxter et al. 2005).

The most important massive magnetite orebodies at Marcona are lensoid to tabular, generally strike northeasterly and dip to the northwest. They are segmented by faults (Fig. 1). Most orebodies exhibit higher Cu grades as well as elevated total sulphide contents at shallow levels. The megascopic forms of the major magnetite and associated dacite bodies are interpreted as formed from comingling intrusive oxide and silicate melts rather than through hydrothermal replacement (Chen et al. 2010b).

Two principal arrays of Cu orebodies have been delimited at Mina Justa, namely the main and upper arrays, both of which are spatially associated with subparallel, northeast-trending and shallowly southeast-dipping faults (Fig. 2). These are 100–200 m apart and 10–200 m in vertical extent (Baxter et al. 2005). The Mina Justa orebodies have massive magnetite–pyrite cores surrounded by hydrothermal breccias, comprising strongly K-feldspar/actinolite/magnetite-altered host rock clasts in a magnetite–sulphide matrix, and in turn surrounded by extensive

magnetite–sulphide veining. Hypogene sulphides in individual orebodies are zoned upwards, and locally laterally, from pyrite–chalcopyrite to bornite–chalcocite ± digenite, with a concomitant increase in Cu grade (Chen et al. 2010a). Late-stage 20- to 50-m-wide andesitic dykes, assigned to the Late Aptian Tunga Andesite Suite (Figs. 1 and 2), cut the orebodies at Mina Justa (Chen et al. 2010a).

Four principal fault systems are identified in the Marcona–Mina Justa area. The oldest, Pista, normal faults strike 295° and dip 60° northeast. The coeval or younger Repetición fault system, which is spatially associated with the Marcona magnetite orebodies, comprises a series of reverse-slip faults which strike 45° and dip 30–60° northwesterly (Fig. 1; Chen et al. 2010a). The main orebodies at Mina Justa are controlled by the Mina Justa faults, with strike directions similar to those of the Repetición Fault system, but with shallow southeast dips and normal displacements. The youngest (Huaca system) normal faults strike 335° and dip 60° to the east and are commonly intruded by the Tunga andesite dykes (Chen et al. 2010a).

Alteration and mineralization

Marcona magnetite deposit

Seven stages of alteration and mineralization are identified at Marcona (Fig. 3a) and summarized herein based on the detailed petrologic and geochronologic studies (Chen et al. 2010a, 2010b). The earliest hydrothermal alteration (stage M-I) generated aggregates of fine-grained, 175–177-Ma-old cummingtonite and coarse-grained, 171 Ma phlogopite (–magnetite) in the upper section of the Marcona Formation, immediately beneath the shallow ocean floor during the initial eruption of the Río Grande andesitic arc. Stage M-II Na metasomatism subsequently affected much of the mine area and is represented by albite and minor Na-rich scapolite. Stage M-III magnetite and stage M-IV magnetite–sulphide mineralization, which together form the massive iron orebodies, comprise a variety of opaque and gangue minerals including magnetite, calcic amphiboles, biotite, phlogopite, K-feldspar, calcite, apatite, diopside and sulphides. Major mineral assemblages assigned herein to stage M-III are magnetite–actinolite (or tremolite ± phlogopite ± apatite) and magnetite–biotite (±actinolite). The main magnetite orebodies have >10-m-wide biotite and K-feldspar alteration selvages in metasedimentary rocks and dacites. Sulphide deposition was initiated at stage M-IV in association with magnetite–actinolite (or tremolite ± calcite) and magnetite–phlogopite (±actinolite or tremolite ± calcite) assemblages. The major sulphides are pyrrhotite, pyrite and minor chalcopyrite, occurring commonly as subhedral to anhedral crystals intergrown with magnetite, silicates and calcite (Chen et al. 2010a).

In stage M-V, sulphide veins, commonly with calcic amphibole, formed in the upper levels of the orebodies and cut massive stage M-III magnetite–calcic–amphibole assemblages. More commonly, stage M-V sulphides and coexisting minerals occur as aggregates in cavities in stage M-III and stage M-IV magnetite–amphibole assemblages. Common stage M-V assemblages include chalcopyrite–pyrite ± pyrrhotite–amphibole and chalcopyrite–pyrite–calcite. Late-stage, M-VII, veins developed in multiple episodes with ambiguous age relationships and include tourmaline–quartz–sulphide, magnetite and sulphide, quartz (±calcite), calcite and hematite (Fig. 3a). Both stages M-V and M-VII represent post-magnetite mineralization hydrothermal activity and contain only minor Cu mineralization.

Mina Justa Cu deposit

Seven stages of hydrothermal alteration and mineralization are also recognized at Mina Justa (Fig. 3b) and summarized herein from the detailed petrological and geochronological studies of Chen et al. (2010a). Stage J-I alteration is

represented by commonly light pink albite and green, fine-grained actinolite replacing plagioclase phenocrysts in andesites. Rocks affected by stage J-II K-feldspar–magnetite alteration are megascopically massive, the K-feldspar commonly occurring as extremely fine-grained crystals replacing plagioclase and the magnetite as fine- to medium-grained aggregates interstitial to K-feldspar. Green to dark green actinolite, assigned to a later stage J-III, generally forms coarse, prismatic crystals which commonly occur as veins cutting stage J-II K-feldspar–magnetite alteration zones or, locally, as the matrix of breccias with clasts of K-feldspar/magnetite-altered host rocks (Chen et al. 2010a). The subsequent deposition of stage J-IV specular hematite is revealed entirely by pseudomorphs of stage J-V magnetite, i.e. “mushketovite”, a major component of stage J-V magnetite–pyrite alteration which generated the massive, lensoid, magnetite bodies which localized the subsequent Cu mineralization and are haloed by magnetite–pyrite veins and hydrothermal breccias. Quartz occurs interstitially to magnetite and pyrite grains in the main magnetite bodies. Other constituents include K-feldspar, chlorite, titanite and fluorine-rich apatite. Stage J-VI Cu sulphide-bearing veins locally cut altered host rocks and stage J-V magnetite–pyrite–quartz assemblages, but, more commonly, Cu sulphides and associated assemblages occur in magnetite–pyrite bodies with microscopic textures indicating the replacement of pyrite and magnetite. The main hypogene Cu sulphides, in order of decreasing abundance, are chalcopyrite, bornite, chalcocite and digenite. Calcite and hematite, locally intergrown with epidote and albite, are directly associated with Cu mineralization (Fig. 3b).

Sampling and analytical techniques

Samples for fluid inclusion microthermometry (Tables 1 and 2) and chemical analysis (Table 3) were chosen based on paragenetic relationships such as those illustrated in Fig. 3 and by Chen et al. (2010a). At Marcona, emphasis was placed on the hydrothermal system from stages M-IV through M-VII, which followed the inferred melt-dominated phases (M-III). Although several minerals were examined, only calcite from stage M-IV, stage M-V and stage M-VII, and quartz from stage M-VII were found to host fluid inclusions amenable to analysis (Table 1 and Fig. 4a–c). At Mina Justa, data were obtained from quartz of stage J-V and calcite of the Cu mineralization stage (J-VI; Table 1 and Fig. 4d, e). Microthermometry was conducted using a Linkam THMS-G-600 heating–freezing stage (–180–600°C), calibrated using Synflinc synthetic fluid inclusion standards (Syn Flint Inc. 1985). The errors associated with temperature measurement below 30°C and above 100°C were ±0.2°C and ±2°C, respectively.

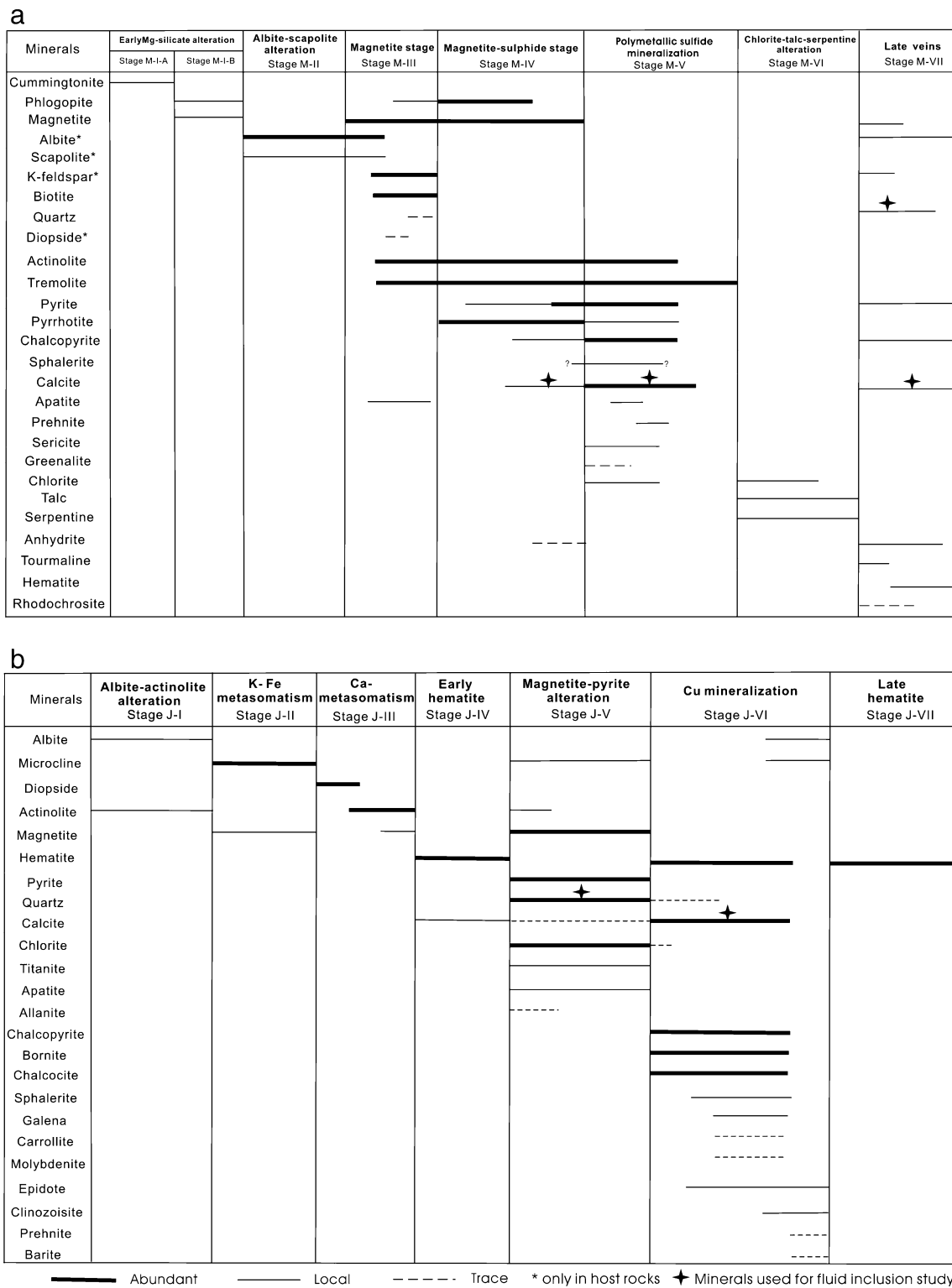


Fig. 3 Alteration and mineral paragenesis of the Marcona (a) and Mina Justa (b) deposits. Supergene minerals omitted

LA-TOF-ICP-MS was chosen for inclusion chemical analysis because it has the ability to quickly analyse numerous elements that results from the opening of a single fluid inclusion by laser ablation. Data were collected

using a Renaissance axial geometry LA-TOF-ICP-MS (LECO Corporation) with 266-nm (UV) laser system under standard operating conditions (0.9- to 1.8-mJ pulse energy, 20-Hz repetition rate, 10- to 150-µm spot size). NIST 612

Table 1 Locations and types of fluid inclusions, Marcona and Mina Justa (paragenetic stages shown in Fig. 3)

| Sample no. | Location | Paragenetic stage | Fluid inclusion hosted minerals | Inclusion types |
|------------|---|-------------------|---------------------------------|------------------------------------|
| MA7-23 | Marcona, Mina 7 open pit; SW corner; 680 m | Stage M-IV | Calcite | U.O. and S; type A (90%)+B (10%)+C |
| DDM4-7-4 | Marcona, drill core DDM4-7; 300 m | Stage M-IV | Calcite | U.O. and S; type A |
| MA2-12 | Marcona, Mina 2 open pit; South side; 650 m | Stage M-V | Calcite | U.O.; type A+D |
| MA2-14 | Marcona; Mina 2 open pit; South side; 650 m | Stage M-VII | Calcite | U.O.; type A |
| MA3-35 | Marcona; Mina 3 open pit; South side; 580 m | Stage M-VII | Quartz | U.O.; type A |
| MA45-3 | Mina Justa; drill core MA45; 267.5 m | Stage J-V | Quartz | U.O.; type A |
| MA89-1 | Mina Justa; drill core MA89; 322.1 m | Stage J-V | Quartz | U.O.; type A (90%)+B (10%)+C |
| MA89-5 | Mina Justa; drill core MA89; 366.5 m | Stage J-VI | Calcite | U.O.; type A (95%)+B-2 (5%) |
| MA27-5 | Mina Justa; drill core MA27; 521.8 m | Stage J-VI | Calcite | U.O.; type A |
| MA17-2 | Mina Justa; drill core MA17; 329.1 m | Stage J-VI | Calcite | U.O.; type A (95%)+B-2 (5%) |

U.O. uncertain origin, *S* secondary

SRM glass (Hinton 1999) was used as an external standard, and concentrations were calculated from the element ratios via an internal standard element, Na, the concentration of which was estimated prior to ablation by microthermometric measurement. The detection limit and error associated with this technique are on the order of 100 ppb and <30%, respectively (Mahoney et al. 1996; Leach and Hieftje 2001; Balcerzak 2003). The high error is generated by calculation of Na concentration from the measured ice melting temperatures. A spatial resolution of up to 10 μm is attained using the laser beam (Olivo et al. 2006). Samples were selected for analysis based on the size of their fluid inclusions and the potential to isolate each inclusion type. At Mina Justa, stage J-V magnetite–pyrite–quartz veins contain the most suitable fluid inclusions for LA-TOF-ICP-MS analysis because of their large size, typically 8–25 μm . In contrast to fluid inclusions in quartz, those in calcite could not be analysed because of the contamination from host ions such as Ca and Mg during the opening of the inclusions and the tendency of calcite to cleave during analysis.

The selection of samples for stable isotope analysis (Tables 4 and 5) was similarly based on detailed petrographic relationships. Pyrite, chalcopyrite, pyrrhotite and molybdenite were chosen for sulphur isotope analysis from the Marcona magnetite–sulphide stage (stage M-IV), the main polymetallic sulphide stage (stage M-V) and the late vein stage (stage M-VII). In addition, sulphide and gypsum (replacing anhydrite) samples were analysed from the Cu/Zn-rich Mina 11, which differs paragenetically from the other orebodies. At Mina Justa, pyrite from the magnetite–pyrite stage (J-V), and bornite and chalcopyrite from the Cu mineralization stage (J-VI) were selected.

Magnetite, amphibole, biotite, apatite and phlogopite from the Marcona magnetite-rich stages (M-III and M-IV) were selected for oxygen isotope analysis, as well as amphiboles from the major sulphide stage (M-V). Magnetite and amphibole from Mina 11 were also selected for comparison. At Mina Justa, magnetite, quartz and apatite from the magnetite–pyrite stage (J-V) were selected for oxygen isotope analysis.

Hydrogen isotope analyses were conducted on stage M-III biotite, amphibole and phlogopite; stage M-IV phlogopite and amphibole; stage M-V amphibole; and stage M-11-I amphibole from Mina 11. Fluids trapped in inclusions in three quartz samples and released by thermal decrepitation were analysed for their hydrogen isotopic compositions. Calcite from the Marcona magnetite–sulphide and major sulphide stages and the Mina Justa Cu mineralization stage IV were analysed for carbon and oxygen isotopes.

Stable isotope analyses were performed at the Queen's Facility for Isotope Research (QFIR). Minerals were extracted from a crushed and washed fraction of the sample or by drilling. Quartz and calcite were selected by handpicking and tested by acid for purity. Magnetite was usually hand picked and concentrated using a magnet. The purity of handpicked silicates was checked by X-ray powder diffraction methods. Both handpicking and drilling were applied on sulphide extraction, but the purity of early-stage pyrite cannot be guaranteed due to the complicated paragenesis at both Marcona and Mina Justa. Sulphur was extracted online with continuous-flow technology, wherein 0.2–0.3 mg of sulphide samples was converted to SO_2 in a Carlo Erba Element Analyzer NCS 2500, with CuO as an oxidant. $\delta^{34}\text{S}$ values are reported relative to Canyon Diablo Troilite standard. Oxygen isotope analysis of silicates and

Table 2 Summary of fluid inclusion petrography and microthermometric data, Marcona and Mina Justa

| Stage | Mineral | Types | Size (μm) | Filling (%) | $T_{\text{homogenization}}$ ($^{\circ}\text{C}$) | | $T_{\text{final ice melting}}$ ($^{\circ}\text{C}$) | | T_{eutectic} ($^{\circ}\text{C}$) | | $T_{\text{final hydrohalite melting}}$ ($^{\circ}\text{C}$) | | n | | | |
|-------------|---------|-----------------|------------------------|-------------|--|-----|---|-------|--|-----|---|-------|-----|-------|-------|----|
| | | | | | Min | Max | Min | Max | Min | Max | Min | Max | | | | |
| Marcona | | | | | | | | | | | | | | | | |
| Stage M-IV | Cal | Type A (U.O.) | 3–20 | 55–75 | 73 | 193 | 123 | –52.2 | –3.1 | 101 | –77.3 | –28.6 | 83 | –49.1 | –45.0 | 3 |
| | | Type A (S.) | 3–9 | 55–75 | 117 | 185 | 29 | –41.1 | –6.0 | 28 | –64.8 | –37.9 | 26 | | | |
| | | Type B-1 (U.O.) | 7–20 | 60–75 | 117 | 220 | 17 | –37.6 | –24.3 | 9 | –65.3 | –43.1 | 9 | | | |
| | | Type B-2 (U.O.) | 7–11 | 20–75 | 102 | 143 | 6 | | | | –41.2 | –41.2 | 1 | | | |
| Stage M-V | Cal | | 4–25 | 50–80 | 75 | 321 | 126 | –31.0 | –0.8 | 88 | –68.1 | –15.0 | 80 | –48.0 | –35.0 | 15 |
| Stage M-VII | Qiz-Cal | | 4–12 | 60–75 | 70 | 170 | 41 | –32.9 | –3.9 | 40 | –57.5 | –8.6 | 38 | | | |
| Mina Justa | | | | | | | | | | | | | | | | |
| Stage J-V | Qiz | Type A (U.O.) | 3–28 | 50–85 | 57 | 374 | 176 | –41.8 | –0.1 | 163 | –87.4 | –16.7 | 128 | –49.7 | –23.7 | 17 |
| | | Type B-1 (U.O.) | 7–25 | 50–75 | 123 | 400 | 12 | –38.1 | –9.0 | 10 | –72.1 | –53.9 | 9 | | | |
| Stage J-VI | Cal | Type B-2 (U.O.) | 7–25 | 50–75 | 96 | 146 | 6 | –30.0 | –21.6 | 5 | –66.6 | –50.0 | 4 | | | |
| | | Type A (U.O.) | 4–30 | 60–80 | 87 | 198 | 107 | –50.4 | –0.4 | 78 | –75.1 | –11.3 | 69 | –45.6 | –37.6 | 8 |
| | | Type B-2 (U.O.) | 4–25 | 60–70 | 88 | 219 | 6 | –49.7 | –22.1 | 3 | –75.6 | –52.1 | 3 | | | |

Cal calcite, Qiz quartz; U.O. uncertain origin, S secondary

Table 3 Average laser ablation time of flight ICP-MS analyses (ppm) of single quartz-hosted fluid inclusions, Mina Justa

| Stage | Types | No. ^{a)} | Fluid features | Li | B | Na | Mg | P | Ca | Mn | Fe | Co | Ni | Cu | Zn | As | Sr | Ba | Mo | Cd | Pb |
|-------|--|-------------------|-------------------------|-----|-------|---------|-----|-------|--------|-----|-------|-----|-----|-------|-----|------|-----|-----|-----|-----|-----|
| J-V | B-1 | 4 | High T, high S, Na-rich | 95 | 1,040 | 112,700 | 97 | 852 | 12,461 | 234 | 3,532 | 26 | 168 | n.d. | 126 | 70 | 73 | 107 | 64 | 26 | 39 |
| J-VI | A | 26 | Low T, high S, Ca-rich | 359 | 811 | 77,799 | 106 | 2,793 | 25,330 | 307 | 5,814 | 57 | 337 | 100 | 483 | 205 | 77 | 181 | 129 | 235 | 105 |
| J-VI | A | 1 | Low T, low S, Na-rich | 397 | n.d. | 38,479 | 14 | 384 | 9,525 | 158 | 485 | 39 | 233 | n.d. | 336 | n.d. | 52 | 37 | 26 | 244 | 5 |
| | Stage J-VI-1 ^{b)} /stage J-V | | | 3.8 | 0.8 | 0.7 | 1.1 | 3.3 | 2.0 | 1.3 | 1.7 | 2.2 | 2.0 | >10.0 | 2.2 | 2.9 | 1.1 | 1.7 | 2.0 | 9.0 | 2.7 |
| | Stage J-VI-2 ^{c)} /stage J-VI-1 | | | 1.1 | 0.0 | 0.5 | 0.1 | 0.1 | 0.4 | 0.5 | 0.1 | 0.7 | 0.7 | 0.0 | 0.7 | 0.0 | 0.7 | 0.2 | 0.2 | 1.0 | 0.1 |

n.d. not detected

^{a)} Number of analyses

^{b)} Stage J-VI-1: low-T, high-salinity and Ca-rich fluid in stage J-VI

^{c)} Stage J-VI-2: Low-T and low-salinity fluid, without Ca

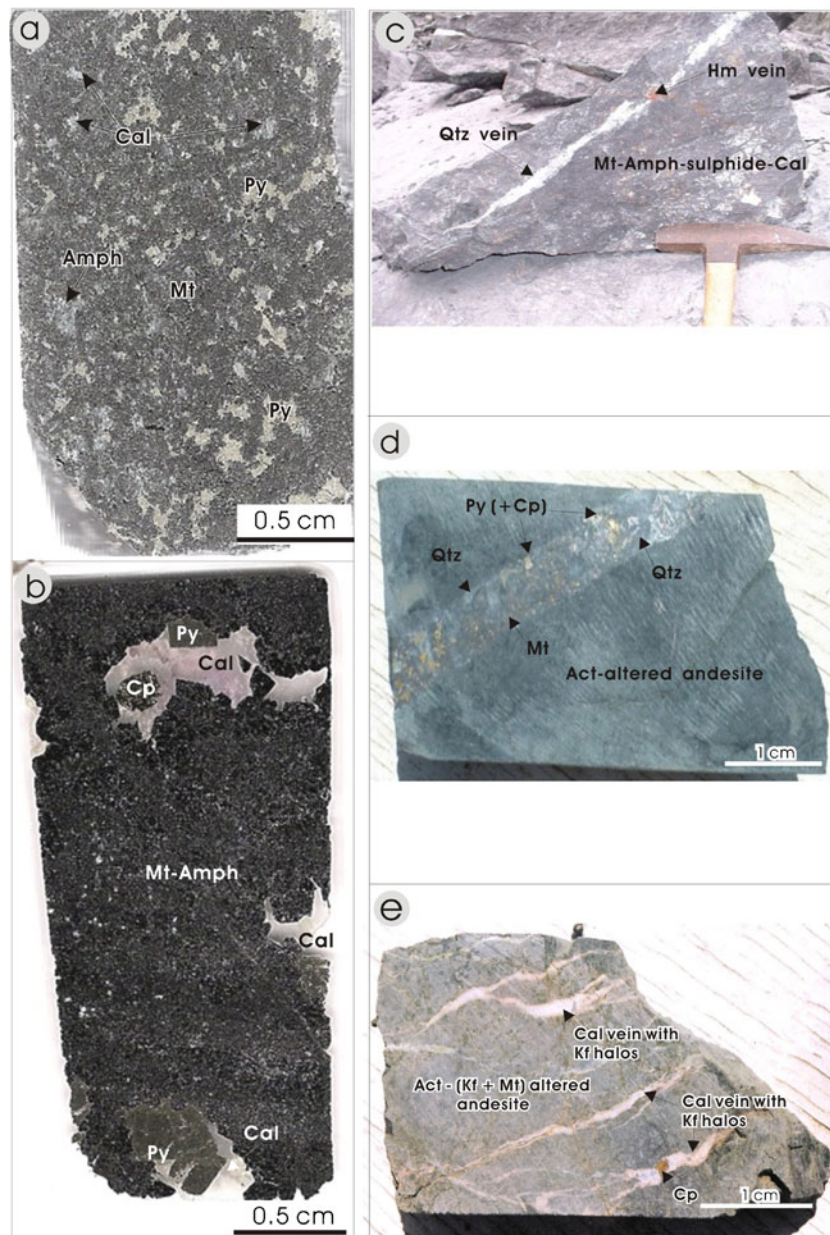


Fig. 4 Mineralogical and textural relationships of fluid inclusion-hosting assemblages from the Marcona and Mina Justa deposits. Marcona: **a** Characteristically fine-grained amphibole (actinolite + tremolite), sulphide and calcite occur interstitially with magnetite in stage M-IV mineralization (#DDM4-7-4, drill core DDM4-7 at 415.1 m, Mina 4 orebody). **b** Stage M-V pyrite, chalcopyrite and calcite occur as aggregates superimposed on stage M-III magnetite (#MA5-3, Mina 5 open pit, 670 m, orebody). **c** Late quartz vein, with erratic calcite and Mn oxides, cuts massive magnetite–amphibole–sulphide assemblages, and is in turn cut by a hematite vein (#MA3-35,

Mina 3 open pit, 580 m, south wall). Mina Justa: **d** Stage J-V Magnetite–pyrite (partly replaced by chalcopyrite)–quartz veins cut actinolite-altered andesite at Mina Justa. Actinolite is chloritized (#MA45-3, drill core MA45, 267.5 m). **e** Stage J-VI chalcopyrite–calcite veins cut actinolite (–K-feldspar–magnetite)-altered andesite. Microcline occurs as haloes around calcite veins and locally cuts calcite (#MA45-6, drill core MA45, 404.2 m). *Amph* amphibole, *Act* actinolite, *Cal* calcite, *Cp* chalcopyrite, *Hm* hematite, *Kf* K-feldspar, *Mt* magnetite, *Py* pyrite, *Qtz* quartz

iron oxides employed the BrF_5 method of Clayton and Mayeda (1963). Hydrogen isotope compositions of quartz-hosted fluid inclusions and silicates were determined using the methods of Kyser and O’Neil (1984). $\delta^{18}\text{O}$ and δD values are reported relative to Vienna Standard Mean Ocean Water (V-SMOW).

$\delta^{18}\text{O}$ and $\delta^{13}\text{C}$ values for carbonate were measured on CO_2 released from 5–10 mg powdered carbonate samples reacted with 100% phosphoric acid using the acid fractionation factor of Sharma and Clayton (1965). The $\delta^{13}\text{C}$ values are reported relative to the V-PDB standard and $\delta^{18}\text{O}$ values to V-SMOW. All isotopes were measured using the QFIR

Table 4 Stable isotopic compositions of minerals from Marcona

| Sample | Stage | <i>T</i> (°C) | $\delta^{34}\text{S}$ | $\delta^{18}\text{O}$ | δD | $\delta^{13}\text{C}$ |
|------------|-------|---------------|--------------------------------------|--|---------------------|-----------------------|
| MA5-9 | M-IA | | | 8.7 (cum) | −62 (cum) | |
| MA5-9 | M-IB | | | 9.4 (phl) | −59 (phl) | |
| DDM 3-3-1 | M-III | 800 | | 4.4 (<i>mt</i>); 8.6 (<i>amph</i>) | −67 (<i>amph</i>) | |
| DDM 3-3-1 | M-III | | | 8.9 (<i>amph</i>) | −63 (<i>amph</i>) | |
| MA3-7 | M-III | 770 | | 4.2 (<i>mt</i>); 8.0 (<i>phl</i>) | −67 (<i>phl</i>) | |
| MA3-22 | M-III | 700–760 | | 3.7 (<i>mt</i>); 7.2 (<i>apt</i>); 8.9 (<i>amph</i>) | −60 (<i>amph</i>) | |
| DDM4-7-1 | M-III | | | 3.9 (<i>mt</i>) | | |
| DDM5-4-7 | M-III | | | 4.6 (<i>mt</i>) | | |
| MA5-9 | M-III | 800 | | 5.2 (<i>mt</i>); 8.7 (<i>bt</i>) | −71 (<i>bt</i>) | |
| MA10-4 | M-III | | | 8.3 (<i>amph</i>) | −64 (<i>amph</i>) | |
| MA3-19 | M-IV | 600 | | 2.9 (<i>mt</i>); 9.3 (<i>phl</i>) | −62 (<i>phl</i>) | |
| DDM 3-3-1 | M-IV | | 3.8 (<i>py</i>) | | | |
| DDM 3-3-1 | M-IV | | 3.7 (<i>py</i>) | | | |
| MA3-8 | M-IV | | 5.9 (<i>py</i>) | | | |
| MA3-18 | M-IV | | 3.9 (<i>py</i>) | | | |
| DDM 4-6-5 | M-IV | 430 | 2.4 (<i>po</i>); 2.1 (<i>cp</i>) | | | |
| DDM 4-7-4 | M-IV | 570 | 1.8 (<i>py</i>) | 13.2 (<i>cal</i>); 4.8 (<i>mt</i>) | | −6.0 (<i>cal</i>) |
| DDM 4-7-10 | M-IV | | | 5.7 (<i>mt</i>) | | |
| DDM 4-7-11 | M-IV | | 2.4 (<i>po</i>) | | | |
| DDM 5-4-3 | M-IV | | 1.2 (<i>py</i>) | | | |
| DDM 5-4-4 | M-IV | | | 3.5 (<i>mt</i>) | | |
| DDM 5-4-5 | M-IV | | 2.6 (<i>py</i>) | | | |
| DDM 5-4-9 | M-IV | | 2.7 (<i>py</i>) | | | |
| MA5-2 | M-IV | | 2.3 (<i>cp</i>) | 4.8 (<i>mt</i>) | | |
| MA5-9 | M-IV | | | 14.5 (<i>cal</i>) | | −7.2 (<i>cal</i>) |
| MA5-10 | M-IV | | 1.9 (<i>py</i>) | 12.9 (<i>cal</i>) | | −8.2 (<i>cal</i>) |
| MA1-9 | M-IV | 590 | 4.0 (<i>py</i>); 3.4 (<i>cp</i>) | | | |
| MA7-13 | M-IV | | | 9.0 (<i>amph</i>) | −64 (<i>amph</i>) | |
| MA7-23 | M-IV | | 2.8 (<i>py</i>) | 11.9 (<i>cal</i>) | | −5.9 (<i>cal</i>) |
| DDM 3-3-1 | M-V | | | 10.5 (<i>amph</i>) | −60 (<i>amph</i>) | |
| DDM 3-3-2 | M-V | | 4.8 (<i>cp</i>) | | | |
| DDM 3-3-5 | M-V | | | 9.0 (<i>amph</i>) | −74 (<i>amph</i>) | |
| DDM 3-3-7 | M-V | | 3.6 (<i>py</i>) | 9.6 (<i>amph</i>) | −63 (<i>amph</i>) | |
| DDM 3-3-8 | M-V | | 0.8 (<i>py</i>) | 9.5 (<i>amph</i>) | −52 (<i>amph</i>) | |
| MA3-8 | M-V | | 5.0 (<i>py</i>) | 14.2 (<i>cal</i>) | | −6.0 (<i>cal</i>) |
| MA3-35 | M-V | | 4.6 (<i>py</i>) | 13.7 (<i>cal</i>) | | −5.0 (<i>cal</i>) |
| MA2-7 | M-V | | | 13.8 (<i>cal</i>) | | −5.0 (<i>cal</i>) |
| MA2-12 | M-V | 360 | 4.7 (<i>py</i>); 3.6 (<i>cp</i>) | 16.5 (<i>cal</i>) | | −5.9 (<i>cal</i>) |
| DDM 4-6-3 | M-V | | 4.6 (<i>py</i>) | | | |
| DDM 4-7-1 | M-V | | 4.0 (<i>py</i>) | | | |
| DDM 4-7-9 | M-V | 160 | 3.5 (<i>py</i>); 2.7 (<i>cp</i>) | | | |
| DDM 5-4-1 | M-V | | | 8.7 (<i>amph</i>) | −62 (<i>amph</i>) | |
| DDM 5-4-2 | M-V | | 2.1 (<i>py</i>) | 8.9 (<i>amph</i>) | −65 (<i>amph</i>) | |
| DDM 5-4-7 | M-V | | | 9.0 (<i>amph</i>) | −60 (<i>amph</i>) | |
| DDM 5-4-8 | M-V | | 3.0 (<i>po</i>) | | | |
| MA5-3 | M-V | | 4.0 (<i>py</i>) | 18.7 (<i>cal</i>) | | −6.8 (<i>cal</i>) |
| MA5-7-2 | M-V | | 1.8 (<i>py</i>) | | | |
| MA7-15 | M-V | | 4.9 (<i>py</i>) | | | |
| DDM 3-3-3 | M-VII | | | 8.6 (<i>mt</i>); 14.5 (<i>cal</i>) ^a | | −5.7 (<i>cal</i>) |

Table 4 (continued)

| Sample | Stage | <i>T</i> (°C) | $\delta^{34}\text{S}$ | $\delta^{18}\text{O}$ | δD | $\delta^{13}\text{C}$ |
|-----------|-------------|---------------|--------------------------------------|-----------------------|------------------------|-----------------------|
| MA3-25 | M-VII | | 7.4 (py \pm cp) | | | |
| MA3-35 | M-VII | | | 14.9 (qtz) | –42 (qtz) ^b | |
| MA2-14 | M-VII | | | 12.3 (cal) | | –5.1 (cal) |
| DDM 4-7-8 | M-VII | | | 13.1 (cal) | | –7.7 (cal) |
| MA7-2 | M-VII | | | 13.7 (cal) | | –6.8 (cal) |
| MA91-3 | M11-I | | | 9.4 (amph) | –61 (amph) | |
| MA91-4 | M11-II | 430 | 2.5 (<i>py</i>); 1.6 (<i>cp</i>) | 4.7 (<i>mt</i>) | | |
| MA91-3 | Early M11-V | | 2.4 (<i>py</i>) | | | |
| MA91-5 | Early M11-V | | 2.6 (<i>mo</i>) | | | |
| MA91-6 | Early M11-V | | 3.9 (<i>py</i>) | | | |
| MA91-3 | Late M11-V | | 15.8 (<i>gy</i>) | | | |
| MA91-5 | Late M11-V | | 14.5 (<i>gy</i>) | | | |

Entries in italics are mineral pairs for geothermometer

ab albite, *amph* amphibole, *apt* apatite, *bn* bornite, *bt* biotite, *cal* calcite, *cc* chalcocite, *cp* chalcopyrite, *cum* cummingtonite, *gy* gypsum, *moly* molybdenite, *mt* magnetite, *phl* phlogopite, *po* pyrrhotite, *py* pyrite, *qtz* quartz

^a Magnetite and calcite in different veins

^b From fluids hosted in fluid inclusions

Finnigan MAT 252 isotope ratio mass spectrometer and are reported in units of per mil (‰). $\delta^{34}\text{S}$, $\delta^{18}\text{O}$, $\delta^{13}\text{C}$ and δD analyses are reproducible to $\pm 0.3\%$, $\pm 0.2\%$, $\pm 0.1\%$ and $\pm 3\%$, respectively.

The isotope fractionation factors used in this study for the calculation of temperatures and fluid compositions are as follows: for sulphur: pyrite–chalcopyrite (Kajiwra and Krouse 1971), pyrrhotite–chalcopyrite (Kajiwra and Krouse 1971); for oxygen: magnetite–quartz (Clayton and Keiffer 1991), magnetite–apatite (Valley 2003), magnetite–H₂O (Bottinga and Javoy 1973), quartz–H₂O (Clayton et al. 1972), calcite–H₂O (O’Neil et al. 1969), amphibole–H₂O (Zheng 1993), biotite–H₂O (Bottinga and Javoy 1973), phlogopite–H₂O (Zheng 1993); for hydrogen: amphibole–H₂O (Suzuoki and Epstein 1976), phlogopite–H₂O (Suzuoki and Epstein 1976), biotite–H₂O (Suzuoki and Epstein 1976); and for carbon: calcite–CO₂ (Ohmoto and Rye 1979).

Results

Fluid inclusions

There is no clear evidence of inclusions being trapped along growth zones in either quartz or calcite crystals from Marcona or Mina Justa, and therefore primary fluid inclusions cannot be identified using the criteria of Roedder (1984) and Goldstein (2003). Many fluid inclusions are distributed in three dimensions in host crystals without

clear crosscutting relationships (Fig. 5a) and fluid inclusion assemblages (Goldstein and Reynolds 1994; Goldstein 2003) cannot be used to distinguish groups of inclusions trapped coevally. These fluid inclusions are uncertain in origin. However, similarly randomly distributed inclusions are inferred to be primary by other authors (e.g. Hedenquist et al. 1998; Wanhainen et al. 2003; Seedorff and Einaudi 2004; Bouzari and Clark 2006), even though their true origin is ambiguous (Bodnar 2003; Goldstein 2003). Locally, unambiguously secondary fluid inclusions are trapped along microfractures cutting crystals (Fig. 5b).

Five fluid inclusion types have been defined on the basis of phases observable at room temperature (Fig. 5c–e): *Liquid–vapour two-phase inclusions* (type A), which account for over 80% of the observed inclusions, contain an aqueous liquid with a vapour bubble. The volumetric liquid/vapour ratio is greater than unity in most inclusions of this type (Fig. 5c). Type A inclusions are predominantly spherical or irregularly shaped and <10 μm in size. All such inclusions homogenize into the liquid phase. *Liquid–vapour–halite three-phase inclusions* (type B-1) contain liquid, a vapour bubble and a halite crystal identified on the basis of its cubic shape, isotropism and refractive index (Fig. 5d). Such inclusions commonly have irregular shapes and are typically <15 μm in diameter. They generally homogenize into the liquid. Type B-2 three-phase inclusions host a daughter mineral other than halite. Some solid phases have medium to high relief and high birefringence and may be an iron chloride or carbonate (Fig. 5e; Smith and Henderson 2000; Bouzari and Clark 2006). Other type

Table 5 Stable isotopic compositions of minerals from Mina Justa

| Sample | Stage | <i>T</i> (°C) | $\delta^{34}\text{S}$ | $\delta^{18}\text{O}$ | δD | $\delta^{13}\text{C}$ |
|--------|-------|---------------|-----------------------|------------------------------------|------------------------|-----------------------|
| MA17-5 | J-V | | 2.6 (py \pm cp) | | | |
| MA17-6 | J-V | | | 3.4 (mt) | | |
| MA35-1 | J-V | | 2.7 (py \pm cp) | | | |
| MA27-2 | J-V | | 2.0 (py \pm cp) | | | |
| MA27-5 | J-V | | | 3.0 (mt) | | |
| MA27-6 | J-V | | 1.1 (py) | | | |
| MA89-1 | J-V | | | 2.7 (mt) ^a ; 13.5 (qtz) | | |
| MA89-2 | J-V | 580 | 1.1 (py \pm cp) | 2.9 (mt); 8.0 (apt) | | |
| MA89-3 | J-V | | 1.7 (py \pm cp) | | | |
| MA89-3 | J-V | | 3.9 (py \pm cp) | | | |
| MA36-1 | J-V | | 1.6 (py \pm cp) | | | |
| MA45-2 | J-V | 540 | 1.7 (py \pm cp) | 3.3 (mt); 9.0 (apt) | | |
| MA45-3 | J-V | 600 | 1.3 (py \pm cp) | 4.7 (mt); 12.6 (qtz) | | |
| MA45-4 | J-V | | 1.6 (py) | 4.4 (mt) | | |
| MA75-2 | J-V | | 0.8 (py \pm cp) | | | |
| MA64-4 | J-VI | | 2.2 (bn \pm cc) | 12.3 (cal) | | -4.4 (cal) |
| MA64-5 | J-VI | | 3.2 (bn) | | | |
| MA17-1 | J-VI | | 1.6 (bn) | | | |
| MA75-1 | J-VI | | 2.0 (bn) | | | |
| MA17-2 | J-VI | | | 13.7 (cal) | | -6.0 (cal) |
| MA17-4 | J-VI | | 2.6 (cp) | | | |
| MA17-8 | J-VI | | 3.7 (cp \pm py) | | | |
| MA17-9 | J-VI | | 3.3 (cp) | 12.2 (cal) | | -7.0 (cal) |
| MA35-1 | J-VI | | | 14.7 (cal) | | -6.9 (cal) |
| MA27-3 | J-VI | | 2.5 (cp \pm py) | 14.3 (cal) | | -6.3 (cal) |
| MA27-5 | J-VI | | 2.7 (cp \pm py) | 14.6 (cal) | | -7.2 (cal) |
| MA89-1 | J-VI | | 1.5 (cp) | | -40 (qtz) ^c | |
| MA89-5 | J-VI | | 2.1 (cp) | 13.3 (cal); 12.6 (ab) ^b | | -7.5 (cal) |
| MA54-2 | J-VI | | 3.7 (cp) | | | |
| MA36-1 | J-VI | | 1.3 (cp \pm py) | | | |
| MA45-3 | J-VI | | 1.7 (cp \pm py) | | -33 (qtz) ^c | |
| MA45-6 | J-VI | | 1.7 (cp) | 13.1 (cal); 13.2 (ab) ^b | | -6.8 (cal) |

Entries in italics are mineral pairs for geothermometer

Abbreviations of minerals as in Table 4

^a Minor hematization in magnetite

^b Albite is relatively late (see Fig. 3) and not in equilibrium with calcite

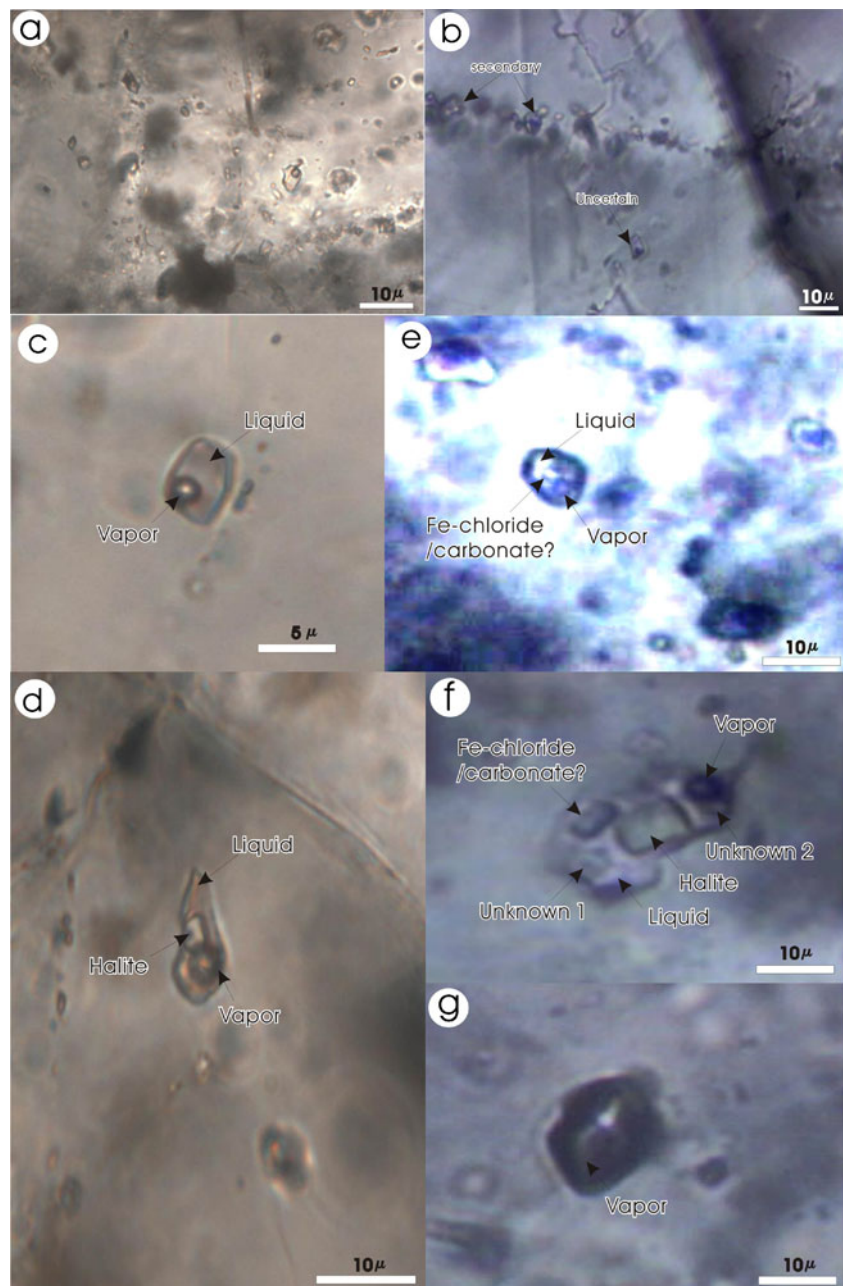
^c From fluids hosted in fluid inclusions

B-2 inclusions have irregular solid phases and variable solid/fluid ratios, and probably record accidental trapping (Goldstein 2003). Rare *multiple-phase* ($n > 3$) inclusions (type C) consist of liquid, a vapour bubble and more than one daughter or accidental mineral, including halite, other salts and solids. Some contain three or four solid phases (Fig. 5f). Dark or transparent *single-phase inclusions* (type D) have rounded and elliptical shapes (Fig. 5g) and show no response to heating or freezing. They are thought to be vapour-dominant (dark) or liquid-dominant (transparent).

These, especially the vapour-rich examples, are generally larger than other types. There is no evidence for liquid CO₂ or clathrates in any inclusions. Inclusion suites showing evidence of boiling were not identified.

Marcona stage M-IV fine-grained calcite interstitial to magnetite and sulphides (Fig. 4a) hosts many distinctly secondary inclusions, although others are randomly distributed and have an uncertain paragenesis. The secondary fluid inclusions are dominantly type A, but the randomly distributed inclusions are mainly type A and type B (B-1-

Fig. 5 Fluid inclusion types in the Marcona and Mina Justa deposits. **a** Fluid inclusions of uncertain origin are randomly distributed in three dimensions (quartz from #MA89-1, drill core MA89, 322.1 m, Mina Justa). **b** Secondary fluid inclusions occur along fractures, some crossing crystal boundaries (calcite from MA7-23, Mina 7 open pit, southwest corner, 680 m, Marcona). **c** Type A: Liquid–vapour two-phase inclusion (quartz from #MA89-1, drill core MA89, 322.1 m, Mina Justa). **d** Type B-1: Liquid–vapour–halite three-phase inclusions (quartz from #MA89-1, drill core MA89, 322.1 m, Mina Justa). **e** Type B-2: Liquid–vapour–non-halite solid three-phase inclusions. The rounded-rhombic solid with high relief and birefringence may be either accidental or a Fe chloride or carbonate daughter mineral (quartz from #MA89-1, drill core MA89, 322.1 m, Mina Justa). **f** Type C: Multiple-phase ($n > 3$) inclusions. At least four solids occur in this inclusion. The cubic, low-relief and low-birefringence daughter mineral is halite. The rhombic, high-relief and high-birefringence daughter may be a Fe chloride or carbonate. Halite melted at 375°C, but the other solids had not homogenized at the 600°C thermal limit of the heating stage (quartz from #MA89-1, drill core MA89, 322.1 m, Mina Justa). **g** Type D: vapour (*dark*) fluid inclusion (calcite from MA2-12, Mina 2 open pit, south side, 650 m, Marcona)



dominant), with a few type C and type D examples (Table 1). Stage M–V coarse-grained calcite (Fig. 4b), however, has no extensive fractures and hosts fluid inclusions which are mainly type A and randomly distributed in three dimensions. Stage M–VII quartz and calcite crystals have no extensive fractures, and the type A fluid inclusions are commonly randomly distributed or isolated, with an uncertain paragenesis.

At Mina Justa, stage J–V quartz crystals, which are pervasively fractured and occur interstitially to magnetite and pyrite, host mainly type A inclusions, with some type B and a few type C. Fluid inclusions in calcite–sulphide veins from the J–VI Cu mineralization (Fig. 4e) are randomly

distributed in three dimensions. Most of these fluid inclusions are type A, whilst the remainder are type B-2 (Table 1).

Microthermometric data representative of host minerals from most alteration–mineralization stages at Marcona and Mina Justa are summarized in Table 2. At Marcona, the majority of type A fluid inclusions in stage M–IV calcite exhibit homogenization temperatures (T_h) of between 73°C and 193°C (Table 2), most falling between 100°C and 140°C (Fig. 6). Secondary type A fluid inclusions from stage M–IV have a similar T_h range and distribution, as do inclusions in calcite from stage M–V and in quartz and calcite from stage M–VII veins (Fig. 6). The similarity in the T_h of inclusions

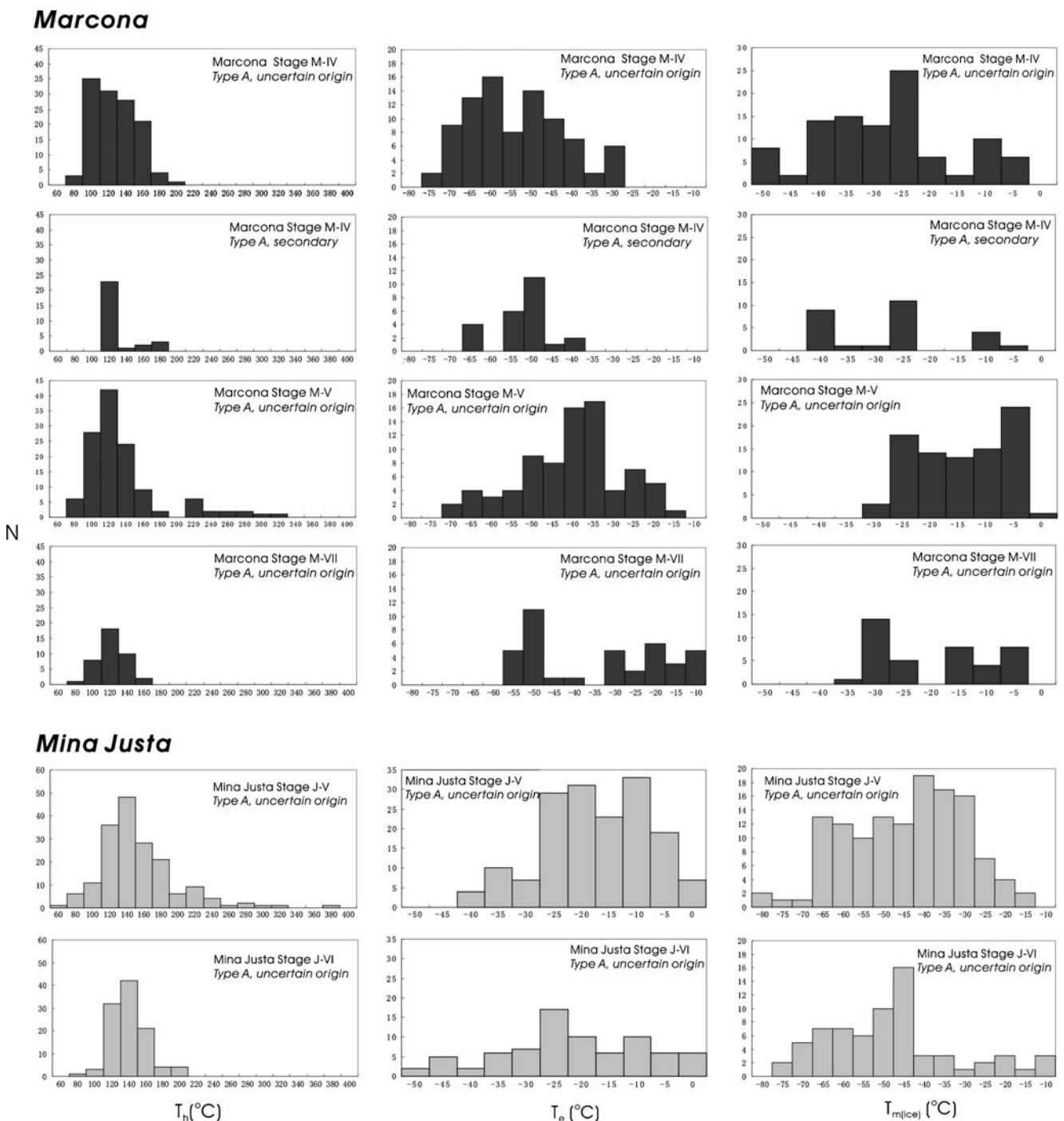


Fig. 6 Histograms of homogenization temperatures (T_h), eutectic temperatures (T_e) and ice melting temperatures ($T_{m(ice)}$) for fluid inclusions in minerals from various paragenetic stages from Marcona and Mina Justa

hosted by mineral assemblages of different mineralization stages implies that all or most of the type A fluid inclusions of uncertain paragenesis in stage M-IV calcite represent fluids trapped at later stages. Trapping of late fluids may also be recorded by inclusions in stage M-V minerals, although no unambiguously secondary inclusions were identified in calcite from this stage. However, the rare higher temperature

($T_h=220\text{--}320^\circ\text{C}$) type A inclusions occur only in stage M-V calcite (Fig. 6).

Type A fluid inclusions of uncertain paragenesis in stage M-IV samples have eutectic temperatures (T_e) between -77.3°C and -28.6°C (Table 2), with modes at -65°C , -50°C and -30°C (Fig. 6). Their ice melting ($T_{m(ice)}$) temperatures range from -52.2°C to -3.1°C , with at least three modes, i.e.

–10°C, –25°C and –40°C (Fig. 6). Secondary type A inclusions in stage M-IV have similar T_c and $T_{m(ice)}$ (Fig. 6), further supporting the secondary paragenesis of the other inclusions. The major T_c and $T_{m(ice)}$ modes of inclusions in stage M-V all appear in stage M-IV inclusions (Fig. 6), but extremely low T_c (–65°C) and $T_{m(ice)}$ (–40°C) values occur only in stage M-IV hosts. Type A (paragenesis uncertain) fluid inclusions in the late veins of stage M-VII have eutectic and ice melting temperatures between –57.5°C and –8.6°C and –32.9°C and –3.9°C, respectively (Table 2). Both T_c and $T_{m(ice)}$ are bimodal and differ from those for stage M-V fluid inclusions which show a T_c peak of –35°C and a $T_{m(ice)}$ peak at –20°C (Fig. 6). However, the possibility that stage M-V calcite trapped low-temperature fluids from stage M-VII cannot be excluded.

Type B fluid inclusions occur only in stage M-IV samples. Of these, type B-1 inclusions have homogenization temperatures between 117°C and 220°C (Table 2), with apparent peaks at 120°C and 200°C. In contrast, type B-2 fluid inclusions, as with both uncertain origin and clearly secondary type A inclusions in stage M-IV (Table 2), have a single peak at 120°C. Consequently, type B-2 and low-temperature type B-1 inclusions are interpreted as secondary, but they are not identified in the subsequent stages M-V and M-VII. The high-temperature (200°C) peak in type B-1 populations may be evidence for another distinct fluid, either a primary stage M-IV fluid or a high-temperature fluid trapped during stage M-V (Fig. 6). First ice melting in type B-1 fluid inclusions occurred at –43.1°C to –65.3°C (Table 2), indicating the presence of Ca or Mg + Fe.

On the basis of geological relationships described by Hawkes et al. (2002), a lithostatic pressure of 1.5–2 kbar, estimated from the overlying 4- to 5-km-thick Río Grande Formation and part of the underlying Marcona Formation (0–1 km), can be inferred for the Marcona magnetite-rich stages (M-III and M-IV). Such pressures entail a correction of approximately 100°C in the estimation of entrapment temperature for the fluid inclusions (Bodnar 2003). Therefore, at Marcona stage M-IV, a highest entrapment temperature of ~300°C is estimated from the plausibly primary fluid inclusions (type B-1, $T_h \leq 220^\circ\text{C}$) hosted by calcite. Although with considerable uncertainty, such temperatures are much lower than those of 430–600°C indicated by sulphur and oxygen isotope geothermometers for this stage (Chen et al. 2010b), which suggests that type B-1 may not represent the stage M-IV primary fluid. However, the temperatures indicated by sulphur isotope geothermometry for stage M-V range from 160°C to 360°C (Chen et al. 2010b), broadly in agreement with the homogenization temperatures of fluid inclusions, which cluster at 120°C with a maximum of 320°C (Table 2 and Fig. 6), indicating a pressure correction for entrapment temperature of <50°C for this stage.

T_h , T_c and $T_{m(ice)}$ data for stage M-V hosted inclusions (all type A with uncertain origin) are plotted in Fig. 7. About 90% of the inclusions have low homogenization temperatures (<200°C) but a wide T_c range, suggesting complex fluid compositions (Goldstein and Reynolds 1994; Fig. 7). On the basis of known stable and metastable eutectic temperatures and observed T_c ranges for various aqueous brine systems (Davis et al. 1990; Goldstein and Reynolds 1994; Baldassarro and Bodnar 2000), the low-temperature fluids may be assigned to Na-rich, Mg/Fe-rich and Ca-rich populations, with Mg/Fe-rich compositions predominating (Fig. 7). The major cations identified from the T_c data are in permissive agreement with the main stage M-V mineral assemblage, i.e. Ca/Mg-rich amphibole + calcite + Fe–Cu sulphides (Fig. 3a). This complex fluid system also exhibits a wide $T_{m(ice)}$ range (Fig. 7), which plausibly indicates a mixture of fluids with varied salinities. Na-dominant fluids, poor in Mg, Fe and Ca, have generally low salinities, whereas the Ca-rich fluids are commonly highly saline and Mg/Fe-rich fluids exhibit both low- and high-salinity populations (Fig. 7). Fluids with moderate salinities are inferred to be products of the mixing of such end-member fluids. Consequently, at least four groups of low-temperature fluids can be recognized in stage M-V, viz., Na-dominant with low salinity, Mg/Fe-rich with low salinity, Mg/Fe-rich with high salinity and Ca-rich with high salinity. Fluids with relatively high homogenization temperatures, i.e. >200°C, observed only in stage M-V calcite, also exhibit wide ranges of composition and salinity (Fig. 7). The limited data, however, preclude the identification of distinct fluid populations.

Type A fluid inclusions of uncertain paragenesis in quartz from the magnetite–pyrite stage (J-V) at Mina Justa have homogenization temperatures ranging widely from 57°C to 374°C (Table 2), with a mode at 140°C (Fig. 6). Fluid inclusions in calcite of the subsequent stage J-VI have T_h values between 87°C and 198°C (Table 2), but again with a 140°C mode (Fig. 6). Eutectic and final ice melting temperatures for both stages J-V and J-VI are characterized by a comparably wide range (Fig. 6). These similarities, as well as the extensively developed fractures in stage J-V quartz, strongly suggest that most type A fluid inclusions in stage J-V quartz are secondary, trapped during the subsequent Cu mineralization. Consequently, the low-temperature inclusions hosted by both stage J-V quartz and stage J-VI calcite may represent the fluids responsible for J-VI Cu mineralization. In contrast, the sparse type A inclusions in stage J-V quartz with high T_h (200–380°C; Fig. 6) are unlikely to represent stage J-VI fluids and may have been trapped at the stage J-V magnetite–pyrite alteration stage. Type B-1 and type C fluid inclusions, which occur only in stage J-V quartz, have homogenization temperatures of between 123°C and 400°C (Table 2), the

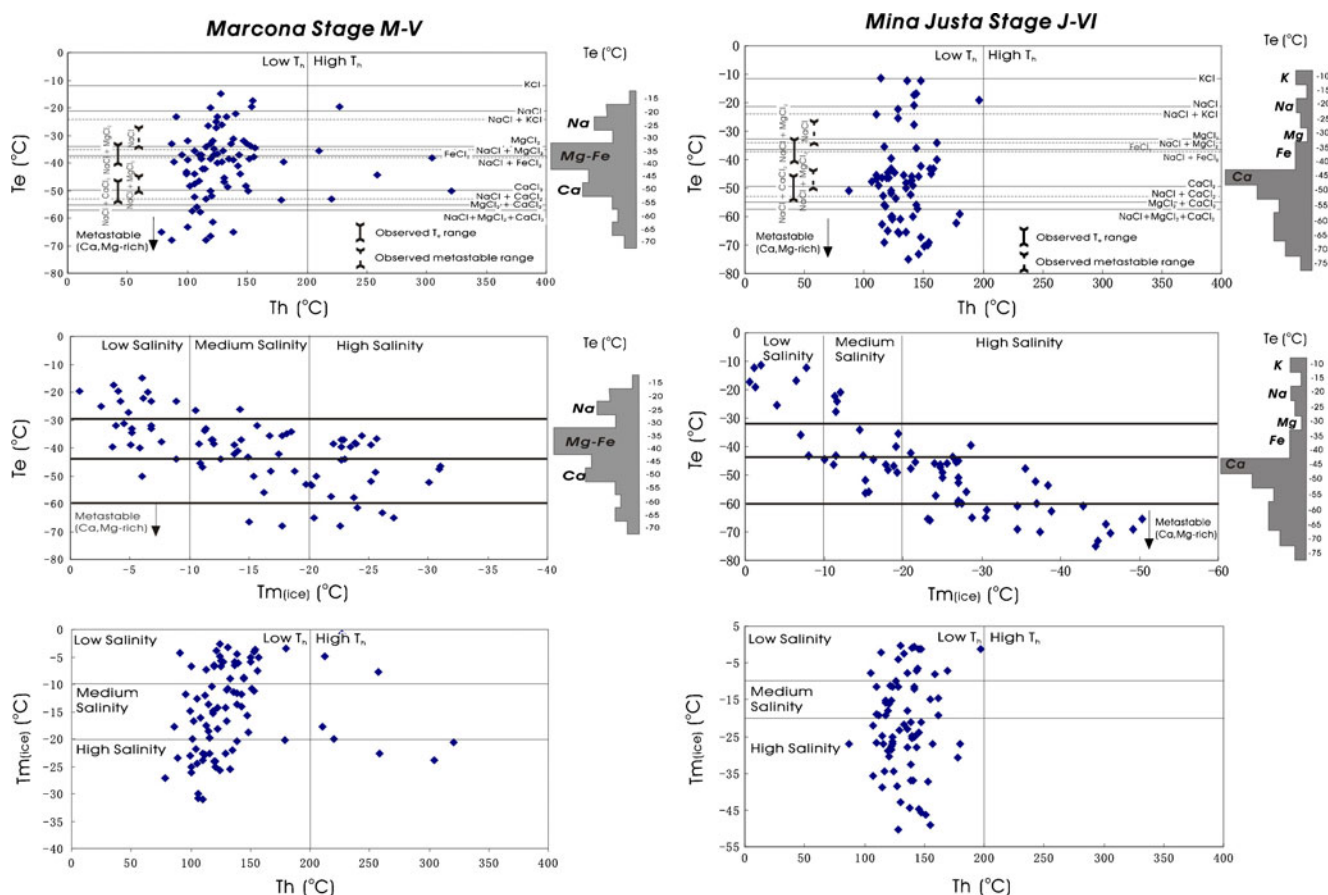


Fig. 7 Relationships among T_e , $T_{m(\text{ice})}$ and T_h for fluid inclusions of the Marcona main sulphide stage (M-V) and Mina Justa Cu mineralization stage (J-VI). The eutectic temperatures of systems with different components are indicated. The observed T_e ranges of the systems NaCl–CaCl₂–H₂O and NaCl–MgCl₂–H₂O, and the observed metastable T_e ranges of the systems NaCl–H₂O and NaCl–MgCl₂–H₂O are shown in T_h vs. T_e space. Lower and higher temperature

populations are divided at 200°C on the basis of homogenization temperatures. Low-, medium- and high-salinity inclusions are differentiated on the basis of final ice melting temperatures ($T_{m(\text{ice})}$) (0°C to –10°C, –10°C to –20°C and less than –20°C, respectively). The histograms of the T_e populations, with inferred dominant cations (see text), are shown on the right

majority exceeding 200°C, indicating that most of the type B-1 (and C) inclusions could be related to the high- T_h type A population, representing primary fluids trapped during stage J-V. Type B-2 inclusions, occurring in both stage J-V quartz and stage J-VI calcite, have low T_h values with a mode at 140°C, similar to those for type A inclusions.

The entrapment pressure for the ore-forming fluids at Mina Justa is uncertain because no boiling fluid inclusions are identified and the stratigraphic load is uncertain. However, on the basis of the pervasive hydrothermal brecciation in the orebodies, the coarse-grained quartz and calcite crystals and the large fluid inclusions (up to 30 μm), a near-surface and hence low-pressure environment is probable and the pressure correction for T_h is probably minor. The maximum T_h determined for the magnetite–pyrite stage (stage J-V) is ~400°C, evidence for an entrapment temperature of at least that value. The temperatures inferred from oxygen isotope geothermometry for

this stage range from 540°C to 600°C (see Table 5), requiring a pressure correction equivalent to ≤ 1 kbar (Bodnar 2003), consistent with the inferred shallow ore-forming environment. The maximum T_h for the later Cu mineralization stage (stage J-VI) is <200°C and most T_h measurements cluster around 140°C, accepted herein as approximating the entrapment temperature.

The Cu mineralization stage (J-VI)-hosted fluid inclusions (mostly type A with a few type B-2) also exhibit eutectic and ice melting temperatures clustering around –45°C to –50°C and –20°C to –25°C, respectively (Fig. 6), which is evidence for a significant Ca content and a high salinity. “Browning” or “orange peel” development (see Goldstein and Reynolds 1994) were commonly observed at the eutectic temperature. Such features were identified in the Olympic Dam deposit by Oreskes and Einaudi (1992) and at Eloise by Baker (1998), where they were also accepted as evidence for Ca-rich ore-forming fluids.

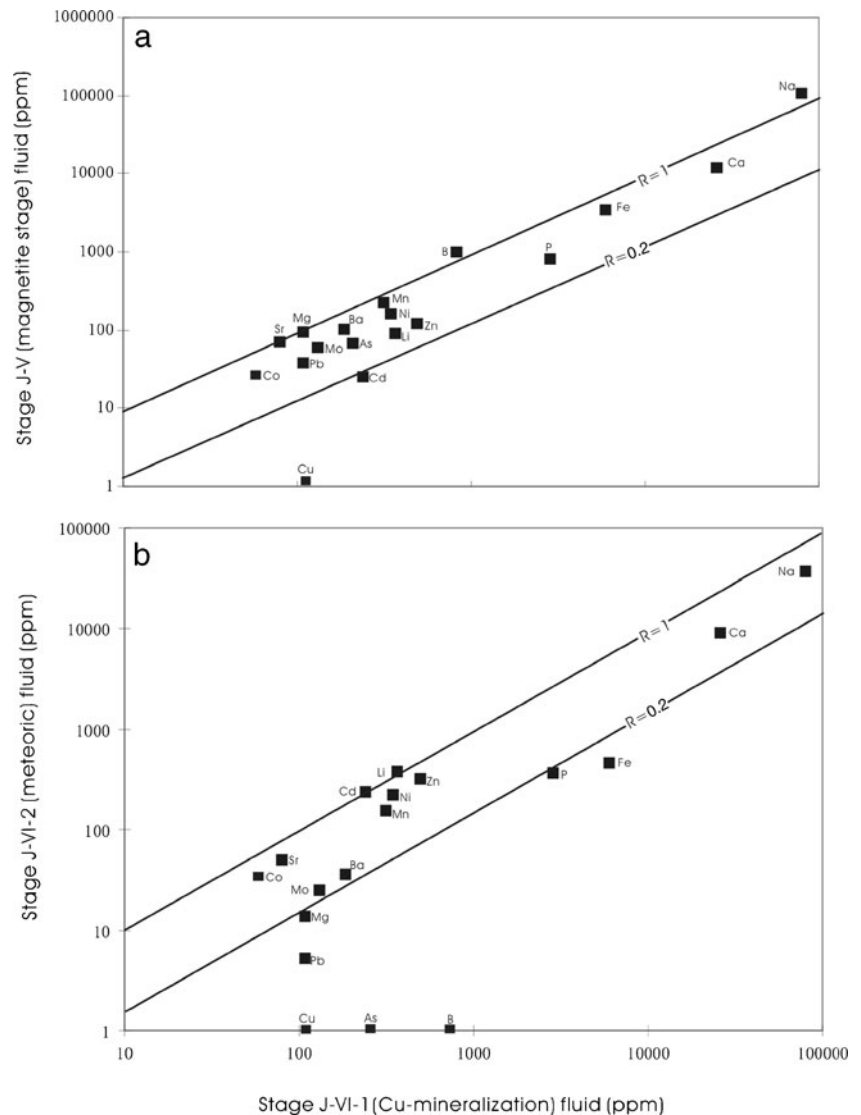
However, the extremely low T_c values (less than -50°C) recorded herein for many fluid inclusions may represent metastable phenomena, which are prevalent in the system $\text{H}_2\text{O}-\text{NaCl}-\text{CaCl}_2$ (Davis et al. 1990). Ca-rich fluids thus apparently dominated the Cu mineralization stage at Mina Justa (Fig. 7). At least two groups of stage J-VI fluids can be identified, viz., Ca-rich with a low temperature and high salinity (stage J-VI-1 in Table 3) and Na (-K)-dominant with a low temperature and low salinity (stage J-VI-2 in Table 3). Other inclusions may record the mixing of these two groups (Fig. 7).

Laser ablation time-of-flight ICPMS results

LA-TOF-ICPMS data were obtained for 31 fluid inclusions hosted by Mina Justa stage J-V quartz. Some major and trace element concentrations have been shown in Table 3. Four type B-1 fluid inclusions with relatively high

homogenization temperatures ($313-400^\circ\text{C}$), such as those which occur only in stage J-V quartz crystals, may represent the primary fluids of the Mina Justa magnetite stage, have high average concentrations of 11.3 wt.% for Na, 1.2 wt.% for Ca and 0.4 wt.% for Fe, in addition to significant B (0.1 wt.%), Ni (169 ppm), Zn (126 ppm) and Ba (107 ppm). In contrast, the ore metals, Cu and Pb, are not detected and are 39 ppm, respectively (Table 3). In comparison, stage J-VI fluid inclusions, interpreted as representing the low-temperature, high-salinity and Ca-rich fluids associated with Cu mineralization (stage J-VI-1 in Table 3 and Fig. 8a), have lower Na (7.8 wt.%) and higher Ca (2.5 wt.%) and Fe (0.6 wt.%) concentrations. They also contain measurable Cu (average of 100 ppm), Zn (483 ppm), Pb (105 ppm) and Mo (129 ppm; Table 3 and Fig. 8a). One low-temperature, low-salinity, and Na/K-dominant fluid inclusion from stage J-VI (Table 3 and Fig. 8b) has much lower contents of Cu and Fe. These data

Fig. 8 **a** LA-TOF-ICP-MS data for average cation concentrations in fluid inclusions of the Mina Justa Cu ore-forming fluid (stage J-VI-1: low-temperature, high-salinity and Ca-rich) and the stage J-V primary fluid. *R* value indicates stage J-V/stage J-VI-1 ratio. **b** Comparison of elemental concentrations in the Mina Justa Cu ore-forming fluid (stage J-VI-1) and in inferred meteoric water (stage J-VI-2: low-temperature, low-salinity and Na-rich). *R* value indicates stage J-VI-2/stage J-VI-1 ratio



strongly suggest that whereas the stage J-V fluids and the probably meteoric fluid involved in stage J-VI were Cu-barren, Cu, Zn, Pb and Mo are markedly concentrated in the stage J-VI low-temperature, high-salinity and Ca-rich fluid.

The LA-TOF-ICP-MS data (Table 3) suggest that although the Na/Ca ratios in stage J-VI Cu mineralization fluid inclusions vary markedly from 1.2 to 24.1 ($n=26$), the majority are below 5.0. In contrast, the Na/Ca ratios estimated from the melting temperature of hydrohalite (T_{hh} , Table 2) and the ice melting temperature in the system $H_2O-NaCl-CaCl_2$ (Oakes et al. 1990) are less than unity, with most below 0.5. Such low estimates may result from the imprecision of T_{hh} measurement, but other cations (e.g. Fe, Zn, Mn, etc.) in the fluids may invalidate the estimation of Na/Ca ratios based on the system $H_2O-NaCl-CaCl_2$.

Figure 9 illustrates the correlations of Na, Ca and Cu with other cations revealed by the TOF data for the Cu mineralization stage J-VI inclusions. Na has a negative or no correlation with most other cations (Fig. 9a, b). Ca is negatively correlated with Na (Fig. 9a), but has a positive correlation with Cu and Zn (Fig. 9c, d). Cu also has a positive correlation with Zn and Co (Fig. 9e, f), in

agreement with the occurrence of sphalerite and carrollite in the Cu-rich assemblages. However, the concentration of each element in contiguous stage J-VI fluid inclusions is variable.

Stable isotope geochemistry

Sulphur, oxygen, hydrogen and carbon isotopic compositions are shown in Tables 4 and 5, incorporating temperatures estimated from S and O isotope geothermometry.

Sulphur isotopic compositions of minerals and hydrothermal fluids

The $\delta^{34}S$ values of Marcona stage M-IV sulphides, intergrown with magnetite, amphibole and trioctahedral micas, range from +0.8‰ to +5.9‰ (Table 6), with a mode at approx. +2‰ (Fig. 10a). The $\delta^{34}S$ values of Marcona stage M-V sulphides, commonly coarse-grained and associated with calcite and amphibole, are more restricted, varying from +1.8‰ to +5.0‰ and clustering near +5‰ (Table 6 and Fig. 10a). One late vein stage (M-VII) pyrite has a $\delta^{34}S$ value of +7.4‰ (Table 6 and Fig. 10a). $\delta^{34}S$

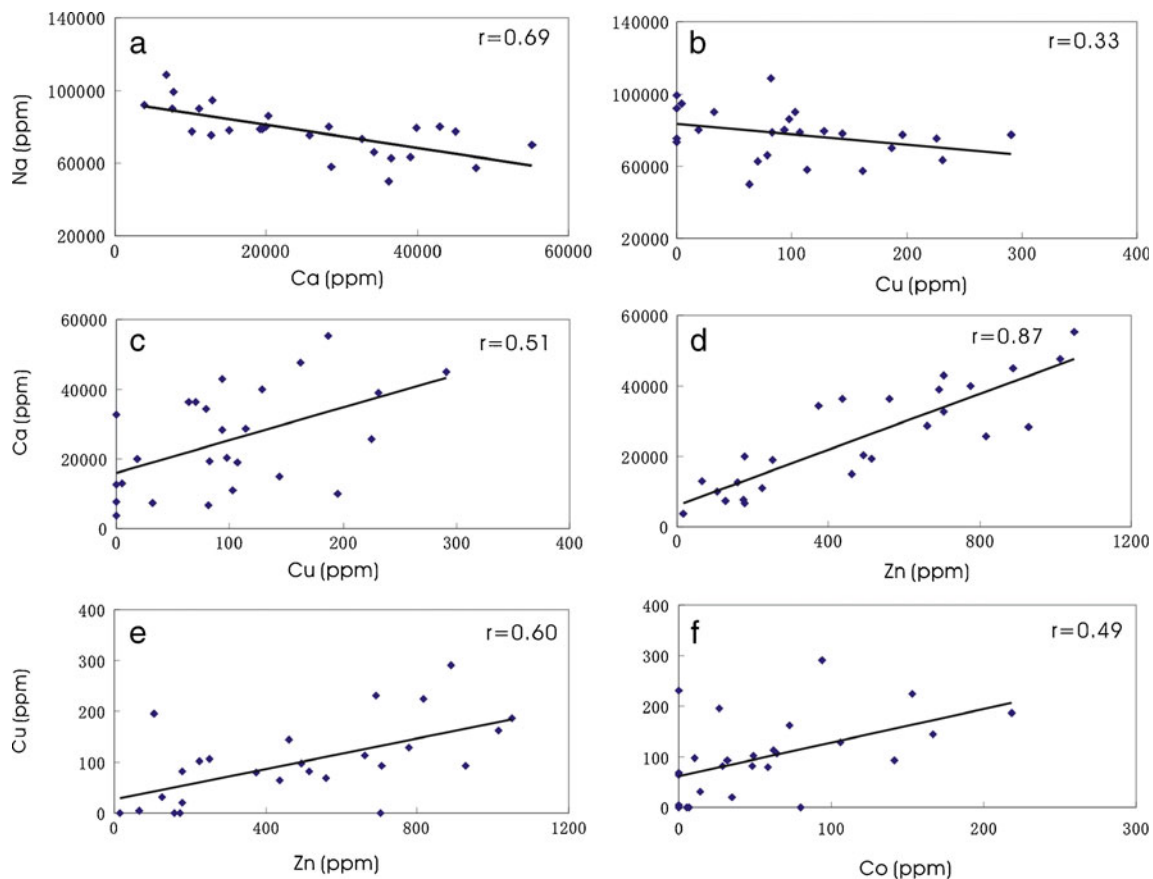


Fig. 9 Inter-element correlations based on all TOF data from Mina Justa stage J-VI. Na versus cations (a and b), Ca versus cations (c and d), Cu versus cations (e and f). r represents correlation coefficient

Table 6 Summary of sulphur isotopic composition of minerals and ore-forming fluids

| Marcona ^a | | | |
|--|--|--|--------------------------------|
| | Magnetite–sulphide stage (M-IV) | Polymetallic sulphide stage (M-V) | Late vein stage (M-VII) |
| $\delta^{34}\text{S}_{\text{sulfides}}$ | +0.8‰ to +5.9‰ ($n=16$) | +1.8‰ to +5.0‰ ($n=17$) | +7.4‰ ($n=1$) |
| Estimated temperature | 430–600°C | 160–360°C | 70–170°C |
| $f\text{O}_2$ indicator | py-cp and po-cp $\delta^{34}\text{S}_{\text{equil}}$; mt-cal $\delta^{18}\text{O}_{\text{equil}}$ | py-cp and po-cp $\delta^{34}\text{S}_{\text{equil}}$ | Fluid inclusions |
| $\Delta = \delta^{34}\text{S}_{\text{H}_2\text{S}} - \delta^{34}\text{S}_{\text{fluid}}$ | Pyrrhotite | Pyrrhotite | Hematite or hematite/magnetite |
| $\delta^{34}\text{S}_{\text{fluid}}$ | 0‰ | 0‰ | Greater than or less than –30‰ |
| $\delta^{34}\text{S}_{\text{fluid}}$ | +0.8‰ to +5.9‰ | +1.8 to +5.0‰ | $\geq 37.4\%$ |
| Mina Justa | | | |
| | Magnetite–pyrite stage (J-V) | Cu mineralization stage (J-VI) | |
| $\delta^{34}\text{S}_{\text{sulfides}}$ | +0.8‰ to +3.9‰ ($n=13$) | +1.3‰ to +3.7‰ ($n=16$) | |
| Estimated temperature | 540–600°C | 88–220°C | |
| $f\text{O}_2$ indicator | mt-qtz and mt-ap $\delta^{18}\text{O}_{\text{equil}}$ | Fluid inclusions | |
| $\Delta = \delta^{34}\text{S}_{\text{H}_2\text{S}} - \delta^{34}\text{S}_{\text{fluid}}$ | Magnetite–pyrite | Hematite | |
| $\delta^{34}\text{S}_{\text{fluid}}$ | 0‰ | Greater than or less than 28‰ | |
| $\delta^{34}\text{S}_{\text{fluid}}$ | +0.8‰ to +3.9‰ | $\geq 29.3\%$ | |

^a $\delta^{34}\text{S}$ values of Mina 11 sulphides and sulphates not included (see text). Abbreviations as in Table 4

values of sulphides from Mina 11 fall into the ranges shown by the other Marcona orebodies (Table 4). Two gypsum samples recording supergene alteration of the Mina 11 anhydrite–sulphide stage (M11-V) have $\delta^{34}\text{S}$ values of +14.5‰ and +15.8‰.

At Mina Justa, pyrite from the magnetite stage (J-V) has $\delta^{34}\text{S}$ values ranging from +0.8‰ to +3.9‰ (Table 6). The $\delta^{34}\text{S}$ values of chalcopyrite and bornite from the ensuing Cu mineralization stage (J-VI) range from +1.3‰ to +3.7‰. Both stage J-V and stage J-VI sulphides have $\delta^{34}\text{S}$ values with modes at approx. +2.0‰ (Fig. 10b).

Given the $f\text{O}_2$ and temperature during mineral precipitation, total $\delta^{34}\text{S}$ values of hydrothermal fluids can be estimated from the $\delta^{34}\text{S}$ values of sulphides and sulphates (Ohmoto and Rye 1979; Ohmoto and Goldhaber 1997). At Marcona, the temperatures determined from sulphur and oxygen isotope geothermometers range from 430°C to 600°C for stage M-IV and from 160°C to 360°C for stage M-V (Table 4). Pyrrhotite occurs in both stages (Fig. 3), evidence for a low $f\text{O}_2$ (pyrite–pyrrhotite buffer in Ohmoto and Rye 1979), and the difference between the $\delta^{34}\text{S}$ values of sulphide and fluids ($\Delta = \delta^{34}\text{S}_{\text{H}_2\text{S}} - \delta^{34}\text{S}_{\text{fluid}}$) would therefore be negligible (Ohmoto and Rye 1979).

The local occurrence of hematite in late veins unaffected by supergene alteration is interpreted as evidence that high $f\text{O}_2$ ($\log f\text{O}_2 \geq -34$ at 250°C and 40 bar; Barton Jr and Skinner 1979) prevailed during stage M-VII. If stage M-VII pyrite was deposited under such conditions, the $\delta^{34}\text{S}$ values of the fluids could have been as high as +37‰, but were probably lower (Table 6). The $\delta^{34}\text{S}$ values of the gypsum from Mina 11 (+14.5‰ and +15.8‰) may represent the $\delta^{34}\text{S}$ values of fluids precipitating anhydrite in this oxidized

environment. However, sulphides from the Cu-rich Mina 11 mineralization stage ($\delta^{34}\text{S}$ values of +1.6‰ to +3.9‰) were probably deposited from fluids having $\delta^{34}\text{S}$ values similar to those in the other Marcona orebodies, on the basis of the temperature of 430°C determined from sulphur isotope geothermometry (Table 4) and the coexistence of magnetite and pyrite, indicating a negligible difference between the $\delta^{34}\text{S}$ values of sulphide and fluids (Ohmoto and Rye 1979).

At Mina Justa, the difference in the $\delta^{34}\text{S}$ values of sulphides and fluids for the magnetite–pyrite stage (J-V) would be negligible at 540–600°C (Table 5) and the moderate $f\text{O}_2$ environment defined by coexisting magnetite and pyrite (Table 6; Ohmoto and Rye 1979). However, fine-grained hypogene hematite is abundant in the Cu mineralization stage (J-VI), indicating a high oxygen fugacity (\geq hematite/magnetite buffer), and the $\delta^{34}\text{S}$ conversion factor for fluids at the low inferred temperatures of 88–220°C is at least –28‰ (Table 6; Ohmoto and Goldhaber 1997), generating $\delta^{34}\text{S}_{\text{fluid}}$ values of $\geq 29.3\%$ (Table 6 and Fig. 10b).

Oxygen isotopic compositions of minerals, melt and hydrothermal fluids

Stage M-III amphibole, biotite and phlogopite have $\delta^{18}\text{O}$ values ranging narrowly between +8.0‰ and +8.9‰, whereas those for stage M-III magnetite vary between +3.7‰ and +5.2‰ (Table 4). Because the main M-III magnetite orebodies are interpreted as having crystallized from a high- T ($\geq 800^\circ\text{C}$, Table 4), iron oxide-dominant hydrous melt which formed through immiscibility from a

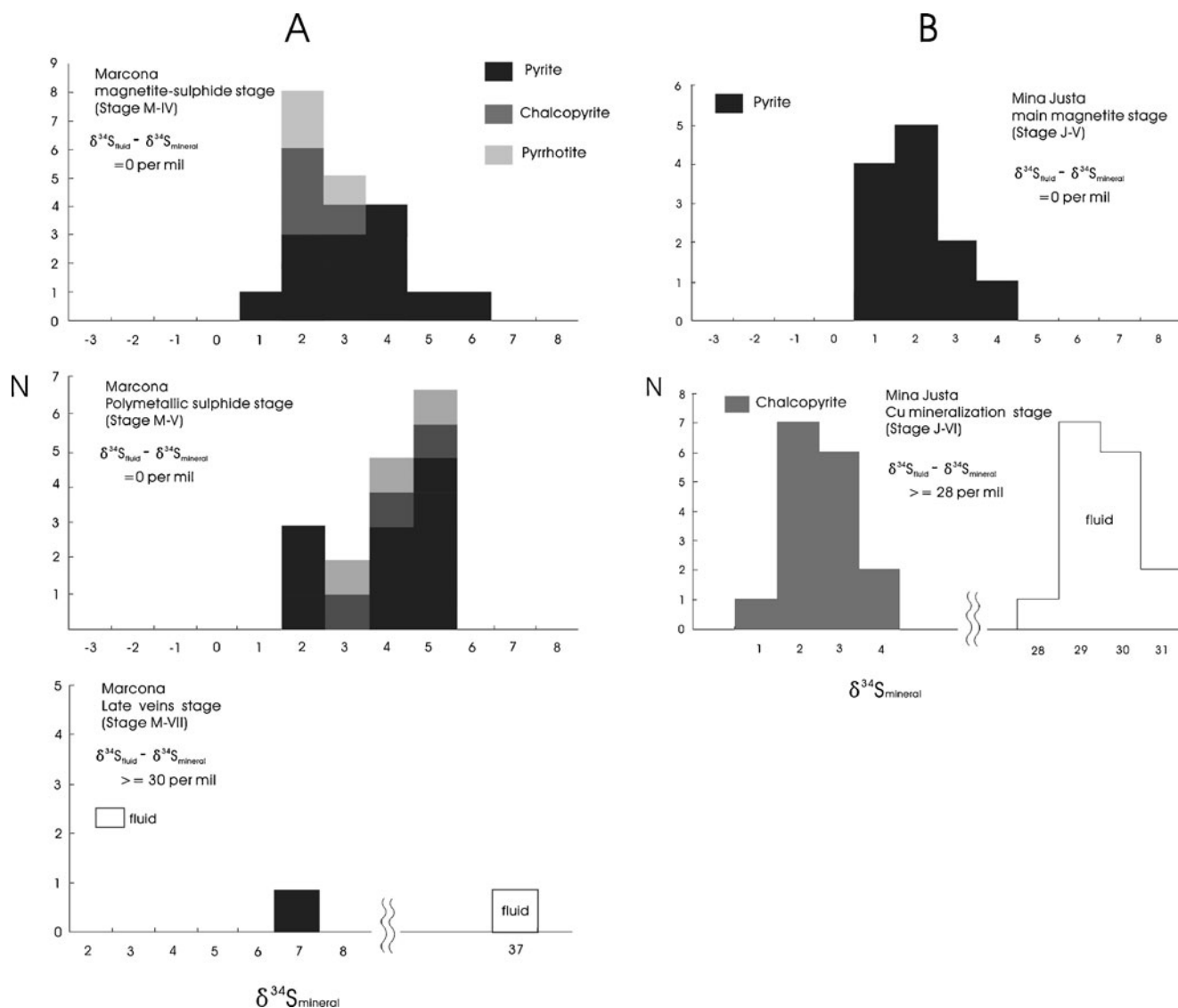


Fig. 10 $\delta^{34}\text{S}$ values of sulphides and calculated ore-forming fluids from Marcona (a) and Mina Justa (b) mineralization and alteration stages

parental andesitic magma (Chen et al. 2010b), isotope exchange factors between minerals and melt, rather than between minerals and water, are probably applicable. Experiments show that ^{18}O preferentially partitions into Si-rich relative to Si-poor minerals with less polymerized structures (Taylor and Epstein 1962). Kyser et al. (1998) demonstrated that a similar fractionation also occurs between Si-rich and Fe-rich immiscible melts. Thus, in the system $\text{Fe}_2\text{SiO}_4\text{-KAlSi}_2\text{O}_6\text{-SiO}_2$ at 1 bar and 1,180°C, the $\delta^{18}\text{O}$ value of a melt with 66.7% SiO_2 and 21.3% FeO was shown experimentally to be 0.6‰ higher than that of a coexisting immiscible Fe-rich melt with 50.1% SiO_2 and 43.5% FeO. The Marcona stage M-III iron oxide-dominant melt would have had an extremely Fe-rich, SiO_2 -poor composition ($\text{SiO}_2 \approx 25\%$, $\text{FeO} \approx 70\%$) from the estimated percentages of minerals and would therefore be predicted to

be strongly ^{18}O -depleted relative to a Si-rich melt (i.e. $\delta^{18}\text{O}_{\text{Si-rich melt}} - \delta^{18}\text{O}_{\text{Fe-rich melt}} \gg 0.6\text{‰}$). Given the $\delta^{18}\text{O}$ values of the Neogene volcanic rocks of the Central Andes, e.g. 6.8–7.4‰ for andesite (Harmon et al. 1984), the $\delta^{18}\text{O}$ value of a potential Marcona oxide melt is inferred to have had a maximum range of 6.2–6.8‰. Furthermore, given the extreme FeO content (~70%) of the Marcona melt, the oxygen fractionation factor between magnetite and inferred melt would have been very small. At 700–800°C (Table 4), a maximum fractionation of 2.5‰ is inferred (Zhao and Zheng 2003) so that on the basis of the $\delta^{18}\text{O}$ values of stage III magnetite, the $\delta^{18}\text{O}$ values of Marcona oxide melt would have had a range of 5.2–7.7‰, in permissive agreement with the estimate based on the data for the Neogene volcanic rocks. Nevertheless, the $\delta^{18}\text{O}$ values of a possible hydrothermal fluid are calculated to be between

8.8‰ and 11.5‰, considering the possibility of magmatic-hydrothermal origin for stage M-III cannot be entirely excluded.

The $\delta^{18}\text{O}$ values of silicates and magnetite from stage M-IV have ranges similar to those of stage M-III, but the associated calcites have higher $\delta^{18}\text{O}$ values, from +11.9‰ to +14.5‰ (Table 4). At temperatures of 570–600°C, as estimated from oxygen isotope geothermometry (Table 4), the $\delta^{18}\text{O}$ values of stage M-IV fluids are inferred to have ranged between +9.6‰ and +12.2‰ (Table 7). The $\delta^{18}\text{O}$ values of coarse-grained stage M-V amphiboles are +8.7‰ to +10.5‰, slightly higher than those of stages M-III and M-IV (Table 4), with those for coexisting calcites varying from +13.7‰ to +18.7‰. At 360°C (Table 4), the calculated $\delta^{18}\text{O}$ values of stage M-V fluids range from +10.1‰ to +12.5‰ (Table 7). Four stage M-VII (late vein) calcites have $\delta^{18}\text{O}$ values of +12.3‰ to +14.5‰, and one vein quartz has a value of +14.9‰ (Table 4). At 120°C (Fig. 6), the $\delta^{18}\text{O}$ values of fluids in equilibrium with the veins would have ranged from -3.6‰ to -1.4‰ (Table 7).

At Mina Justa, $\delta^{18}\text{O}$ values of stage J-V magnetite lie between +2.7‰ and +4.7‰, and two quartzes have values of +12.6‰ and +13.5‰ (Table 5). The calculated $\delta^{18}\text{O}$ values of 540–600°C (Table 5) fluids in stage J-V range between +9.5‰ and +11.5‰ (Table 7). These $\delta^{18}\text{O}$ values are similar to those of the fluids of the Marcona magnetite-sulphide stage (stage M-IV). Calcites from the Cu mineralization stage (J-VI) have $\delta^{18}\text{O}$ values between +12.2‰ and +14.7‰. At 140°C (Fig. 6), an average $\delta^{18}\text{O}$ value of 0.1‰ is calculated for the ore-forming fluids (Table 7).

Hydrogen isotopic compositions of silicates, melt and fluids

The δD values of Marcona stage M-III amphiboles range from -67‰ to -62‰, whereas M-III phlogopite gives a δD value of -67‰ and a biotite a value of -71‰ (Table 4). These data probably record the hydrogen isotope chemistry of the inferred oxide melt. At 700–800°C, the calculated δD values of the melt vary between -73‰ and -43‰ (Table 7). A phlogopite from later stage M-IV has δD value of -62‰

Table 7 $\delta^{18}\text{O}$, δD and $\delta^{13}\text{C}$ values of minerals and fluids from various stages at Marcona and Mina Justa

| Stages | Minerals | $\delta^{18}\text{O}$ | δD | $\delta^{13}\text{C}$ | T (°C) | $\delta^{18}\text{O}_{\text{fluid}}$ | $\delta\text{D}_{\text{fluid}}$ | $\delta^{13}\text{C}_{\text{fluid}}$ |
|------------|----------|-----------------------|------------------|-----------------------|------------------|--------------------------------------|---------------------------------|--------------------------------------|
| Marcona | | | | | | | | |
| M-III | amph | 8.6 (1) ^a | -67 (1) | | 800 ^b | 5.2–7.7 ^f | -54 | |
| | bt | 8.7 (1) | -71 (1) | | 800 ^b | | -50 | |
| | phl | 8.0 (1) | -67 (1) | | 770 ^b | | -73 | |
| | amph | 8.9 (1) | -60 (1) | | 700 ^b | | -43 | |
| | mt | 4.2 (5) | | | 770 ^c | | | |
| M-IV | phl | 9.3 (1) | -62 (1) | -6.0 (1) | 600 ^b | 11.7 | -60 | -3.3 |
| | cal | 13.2 (1) | | | 570 ^b | 12.2 | | |
| | mt | 3.9 (2) | | | 590 ^b | 9.6 | | |
| M-V | cal | 16.5 (1) | | -5.9 (1) | 360 ^b | 12.5 | | -3.4 |
| | amph | 9.3 (7) | -60 (7) | | 360 ^d | 10.1 | -8 | |
| M-VII | qtz | 14.9 (1) | | | 120 ^e | -3.6 | -42 ^g | |
| | cal | 13.7 (4) | | -6.3 (4) | 120 ^e | -1.4 | | -9.2 |
| Mina Justa | | | | | | | | |
| J-V | qtz | 12.6 (1) | | | 600 ^b | 11.5 | | |
| | mt | 3.7 (3) | | | 570 ^c | 9.5 | | |
| J-VI | cal | 13.5 (8) | | -6.4 (8) | 140 ^e | 0.1 | | -8.3 |
| | qtz | | | | | | -37 (2) ^g | |

Abbreviations of minerals as in Table 4

^a Value (number of analyses)

^b Temperature estimated by isotope geothermometry from the sample

^c Average temperature attained by geothermometry

^d Temperature estimated by geothermometry from other samples assigned to this stage

^e Temperature estimated by microthermometry

^f $\delta^{18}\text{O}$ values are estimated for stage M-III oxide melt (see text for discussion)

^g From fluid inclusions hosted by quartz

(Table 4), which at 600°C indicates that stage M-IV fluids had a δD value of -60‰ (Table 7). Stage M-V coarse-grained amphibole samples give a range of δD values between -74‰ and -52‰ (Table 4), corresponding at 360°C to a δD_{fluid} value of -8‰ (Table 7). Fluid trapped in fluid inclusions hosted by a late stage M-VII quartz vein has a δD value of -42‰ (Table 7).

At Mina Justa, δD values of -32‰ and -40‰ (average -37‰) were determined for two samples of fluid inclusions hosted by stage J-V quartz (Table 7). However, paragenetic relationships and fluid inclusion petrography imply that these values record the hydrogen isotopic composition of the subsequent Cu mineralization fluids (stage J-VI).

Carbon isotopic compositions of calcites and hydrothermal fluids

The $\delta^{13}\text{C}$ values of stage M-IV calcites from Marcona range between -8.2‰ and -5.9‰ and those of stage M-V calcites from -6.8‰ to -5.0‰ (Table 4). The fractionation factor for calcite– CO_2 determined by Ohmoto and Rye (1979) indicates that at 570°C, the $\delta^{13}\text{C}$ value of Marcona stage M-IV fluids was -3.3‰ . A similar value (-3.4‰) is estimated for stage M-V 360°C fluids (Table 7). Calcite samples from late barren veins (stage M-VII) have $\delta^{13}\text{C}$ between -7.7‰ and -5.1‰ , so that the average $\delta^{13}\text{C}$ value of stage M-VII $\sim 120^\circ\text{C}$ fluids was -9.2‰ , generally lower than those of stage M-IV and M-V fluids (Table 7).

At Mina Justa, the $\delta^{13}\text{C}$ values of eight calcites from the Cu mineralization stage fall between -7.5‰ and -4.4‰ , similar to those of Marcona calcite (Table 5). However, at 140°C, the average $\delta^{13}\text{C}$ value of the ore-forming fluid would have been -8.3‰ , differing significantly from those

of Marcona stage M-IV and stage M-V fluids, but similar to those of stage M-VII late vein fluids (Table 7).

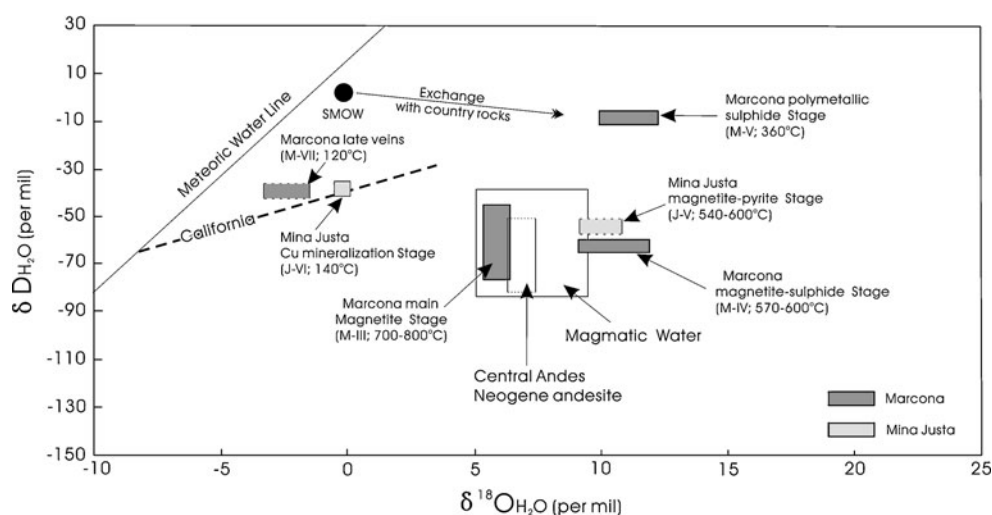
Discussion

Fluid evolution in the Marcona deposit

Oxygen isotope geothermometers give temperatures of 700–800°C for the sulphide-barren magnetite stage III which dominates the Marcona deposit. The $\delta^{18}\text{O}$ and δD values estimated for the inferred stage M-III oxidic melt plot within the magmatic water range, and close to those characteristic of Central Andean Neogene andesite (Fig. 11). A magmatic source for stage M-III is also indicated by the relationships between $\delta^{18}\text{O}$ and temperature (Fig. 12), which are distinct from those of other documented, unambiguously hydrothermal IOCG deposits (e.g. Olympic Dam, Ernest Henry and La Candelaria), but similar to those of Central Andean Neogene dacitic and andesitic magmas (Fig. 12). The $\delta^{18}\text{O}$ values of stage M-III magnetite (3.7–5.2‰, Table 4) are comparable to those of magnetite from El Laco (3.6–4.6‰; Rhodes et al. 1999), an iron oxide deposit inferred to be of melt origin by some (Naslund et al. 2002), but hydrothermal by others (Rhodes et al. 1999; Sillitoe and Burrows 2002).

The inferred primary fluid inclusions hosted by Marcona stage M-IV calcite have moderate homogenization temperatures (up to 220°C) and are commonly highly saline, with varied cationic compositions. Sulphur and oxygen isotope geothermometers indicate a temperature range of 430–600°C (Table 4). Stage M-IV fluids have $\delta^{18}\text{O}$ and δD values that plot close to the magmatic water field (Fig. 11). Fluids at this stage also exhibit similarities in temperature and oxygen isotopic composition to those identified at Ernest

Fig. 11 Calculated δD and $\delta^{18}\text{O}$ values of fluids at Marcona and Mina Justa. Fields for magmatic waters are from Taylor (1997) and for Neogene andesites of the Central Andes from Harmon et al. (1984). The trajectories for seawater (SMOW) exchange with host rocks are from Ripley and Ohmoto (1977). The deviation of the δD and $\delta^{18}\text{O}$ values (dashed line) from the meteoric water line represents formation water of the Kettleman North Dome basin from California (Longstaffe 1987)



Henry (Mark et al. 2000) and for the early, Cu (Au)-barren magnetite stages at Olympic Dam (Oreskes and Einaudi 1992), which are inferred to be of magmatic–hydrothermal origin (Fig. 12). The $\delta^{34}\text{S}$ values of stage M-IV fluids and sulphides fall in a narrow range from +0.8‰ to +5.9‰ (mode at ~2.5‰), indicating a magmatic source (Nielsen 1979). These data are comparable to those documented from some major IOCG deposits, which have $\delta^{34}\text{S}_{\text{sulphide}}$ values of $0\pm 5\%$ (Fig. 13; Williams et al. 2005). Furthermore, the calculated $\delta^{13}\text{C}$ and $\delta^{18}\text{O}$ values of the fluids in stage M-IV are similar to those of magmatic CO_2 (Fig. 14; Taylor 1986; Javoy et al. 1988). The dacite magma around magnetite bodies may have been the source of the magmatic–hydrothermal fluids at this stage (Fig. 15).

The fluids responsible for stage M-V were apparently diverse (Fig. 7). Higher temperature ($T_h=200^\circ\text{C}$ to $\geq 320^\circ\text{C}$), Na-rich/low-salinity and Ca-rich/high-salinity groups were probably magmatic in origin, although the reason for variable composition is unclear, whereas the low-temperature (~120°C) populations record mixing of meteoric water (low-salinity and Na-rich) with modified seawater (Mg/Fe-rich or Ca-rich, medium to high salinities), the latter being the product of reactions between seawater and Ca-rich andesite and metasediments (Fig. 15c). IncurSION of external fluids during stage M-V is also supported by oxygen and hydrogen isotopic compositions, which are distinct from those of the magmatic fluids of stage M-III and stage M-IV (Fig. 11), and apparently record a shift away from magmatic compositions with decreasing temperature (Fig. 12). Callovian–Oxfordian ande-

sites of the Upper Rio Grande Formation erupted in a shallow marine environment (Caldas 1978; Aguirre 1988). Metamorphic fluids, with temperatures of ~250°C, probably derived from the reaction of seawater with hot andesite (Aguirre 1988) or intense heat flow during the initial development of a basin (i.e. diastothermal processes: Alt 1999), generated extensive alteration. Modified seawater was also identified in the mineralization stage at Raúl-Condestable, 300 km NNW of Marcona (Fig. 11; Ripley and Ohmoto 1977) and may have contributed to stage M-V sulphide precipitation. However, the $\delta^{34}\text{S}$ values of the fluid may have been modified through water/rock reaction (Bowers 1989). Jurassic seawater, which generally had $\delta^{34}\text{S}$ values of 16‰ (Hoefs 1997), is inferred to have interacted with andesite and basaltic andesite ($\delta^{34}\text{S}$ values ~0‰), generating a fluid with low $\delta^{34}\text{S}$ values (1.8–5.0‰, Table 6). Calculated $\delta^{13}\text{C}$ and $\delta^{18}\text{O}$ values of fluids for Marcona stage M-V at 360°C fall in the magmatic range (Fig. 14), but may record the involvement of seawater ($\delta^{13}\text{C}=0\%$, $\delta^{18}\text{O}=0\%$; Hoefs 1997), with high $\delta^{18}\text{O}$ and low $\delta^{13}\text{C}$ values as the result of reaction with intermediate-to-mafic volcanic rocks (average $\delta^{13}\text{C}$ values -10‰ to -5‰; $\delta^{18}\text{O}$ values +8‰ to +10‰; Hoefs 1997).

Fluid evolution in the Mina Justa deposit

The inferred primary fluid inclusions hosted by Mina Justa stage J-V quartz have high homogenization temperatures ($T_h\leq 400^\circ\text{C}$), high salinities and variable cationic compositions. Oxygen isotope geothermometers indicate temper-

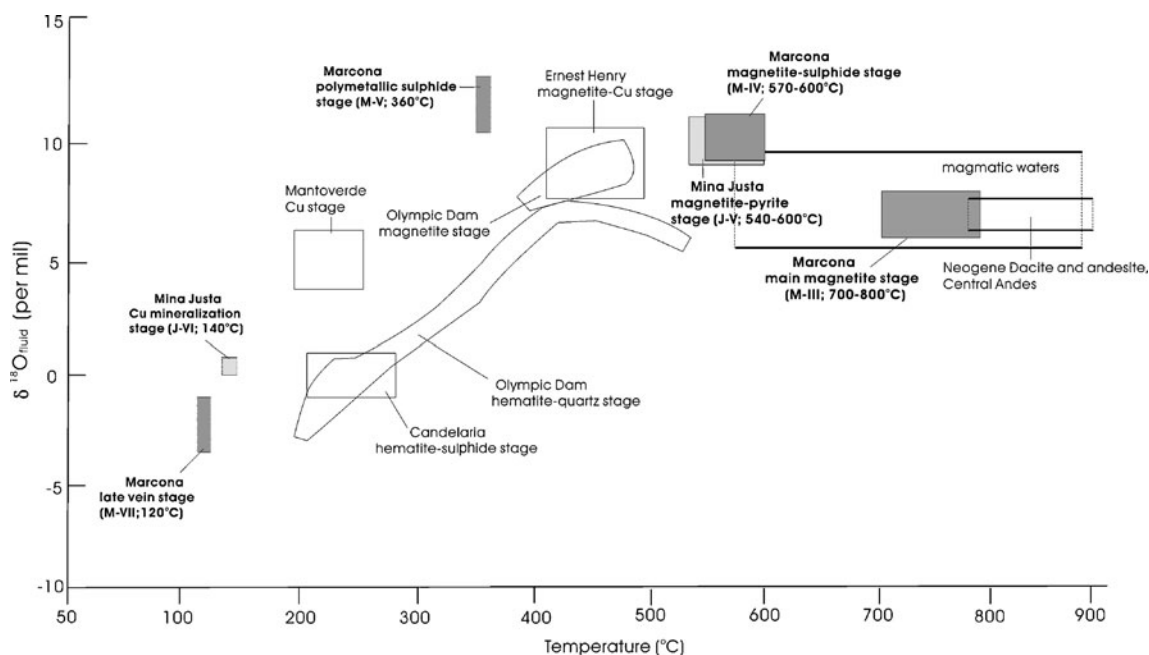


Fig. 12 $\delta^{18}\text{O}_{\text{fluid/melt}}$ -temperature relationships for main mineralization and alteration stages at Marcona and Mina Justa and other IOCG deposits (data for Mantoverde from Benavides et al. 2007; other data

from Williams et al. 2005 and references therein). Magmatic water and Neogene Andean dacite and andesite fields are from Taylor (1997) and Harmon et al. (1984)

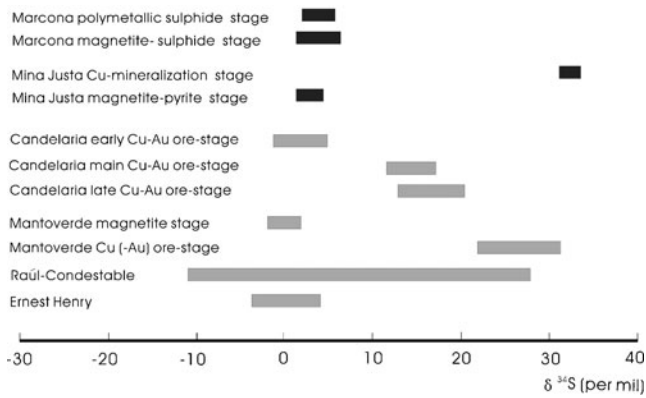
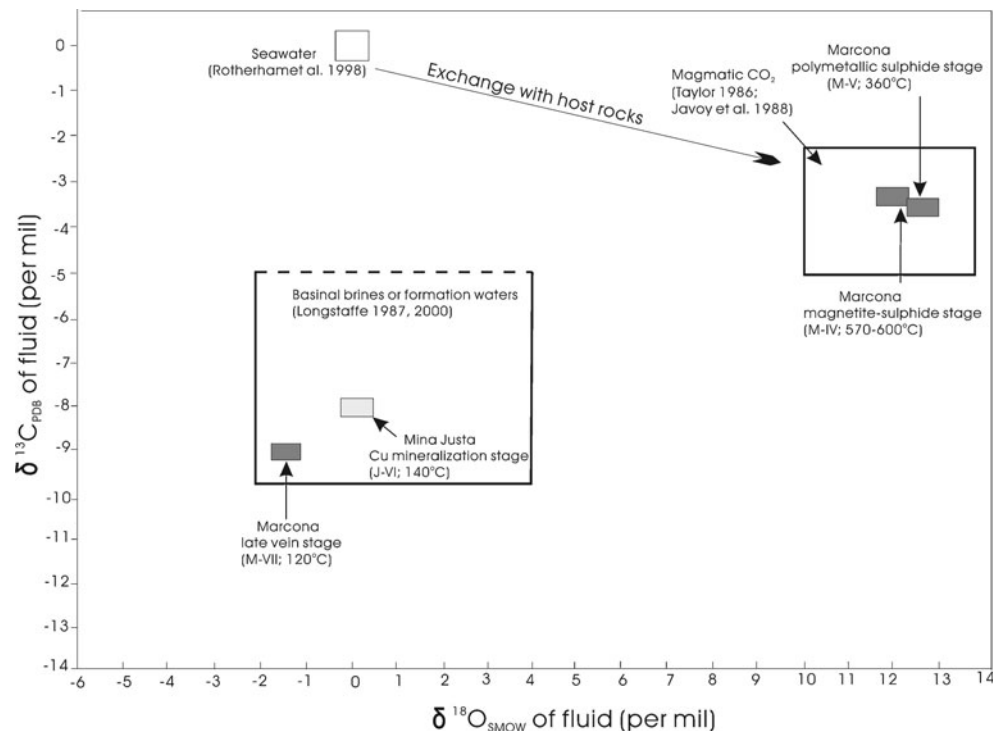


Fig. 13 $\delta^{34}\text{S}$ values of ore fluids at Marcona and Mina Justa and other major IOCG deposits (data from Ullrich and Clark 1999; de Haller et al. 2002; Benavides et al. 2007; Williams et al. 2005 and references therein)

atures of 540–600°C, similar to that of the Marcona magnetite–sulphide stage (M-IV). The $\delta^{18}\text{O}$ and δD values estimated for stage J-V plot close to the magmatic water field (Fig. 11), again comparable to Marcona stage M-IV fluids. A magmatic source for stage J-IV is also indicated by the relationship between $\delta^{18}\text{O}$ and temperature (Fig. 12), wherein the stage J-IV values are similar to those of the Marcona stage M-IV and other IOCG deposits inferred to be of magmatic–hydrothermal origin. The $\delta^{34}\text{S}$ values of stage J-V sulphides and fluids fall in a narrow range between +0.8‰ and +3.9‰ (Fig. 13), similar to those of Marcona stage M-IV and evidence for a dominant magmatic source (Nielsen 1979).

Fig. 14 Calculated $\delta^{13}\text{C}$ and $\delta^{18}\text{O}$ values of hydrothermal fluids, Marcona and Mina Justa mineralization and alteration stages



The $^{40}\text{Ar}/^{39}\text{Ar}$ ages for stage J-V hydrothermal microclines (101–104 Ma; Chen et al. 2010a) coincide with the initial emplacement of the Coastal Batholith in the Acarí area to the east, i.e. $\leq 109 \pm 4$ Ma (Vidal et al. 1990). Small granodiorite–diorite stocks crop out ~3 km east of Mina Justa (Fig. 16a), supporting a genetic relationship between stage J-V magnetite–pyrite alteration and the Coastal Batholith. Magmatic–hydrothermal fluids may have risen along the ENE-striking Mina Justa normal faults which controlled the emplacement of the Fe and Cu orebodies (Fig. 16a).

Fluids documented for the Cu mineralization stage are mainly low-temperature (~140°C), high-salinity and Ca-rich, but with a minor low-temperature, low-salinity and Na-dominant component. The former is inferred to be a Ca-rich basinal brine and the latter is probably meteoric water. LA-TOF-ICP-MS analyses indicate that Cu and other ore metals are restricted to the Ca-rich fluids, i.e. the exotic brines, both the high-temperature primary fluids at stage J-V (magnetite stage) and the meteoric water being Cu-barren. The mineralizing stage J-VI fluids differ also markedly from those of magnetite stage in their lower temperatures and $\delta^{18}\text{O}$ values (Fig. 12) and are unlikely to have been of magmatic derivation. Such non-magmatic fluids were also involved in the hematite-rich mineralization stages at Olympic Dam district (Oreskes and Einaudi 1992; Haynes et al. 1995; Bastrakov et al. 2007), La Candelaria (Ullrich et al. 2001) and Mantoverde (Benavides et al. 2007). A non-magmatic model for Cu mineralization is supported by the relationships between $\delta^{18}\text{O}$ and δD

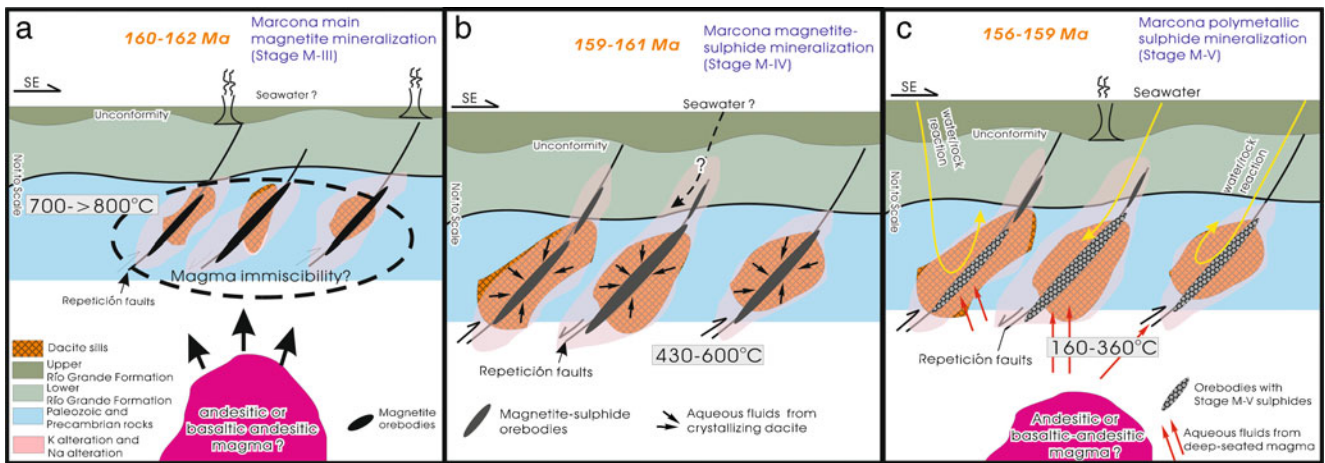
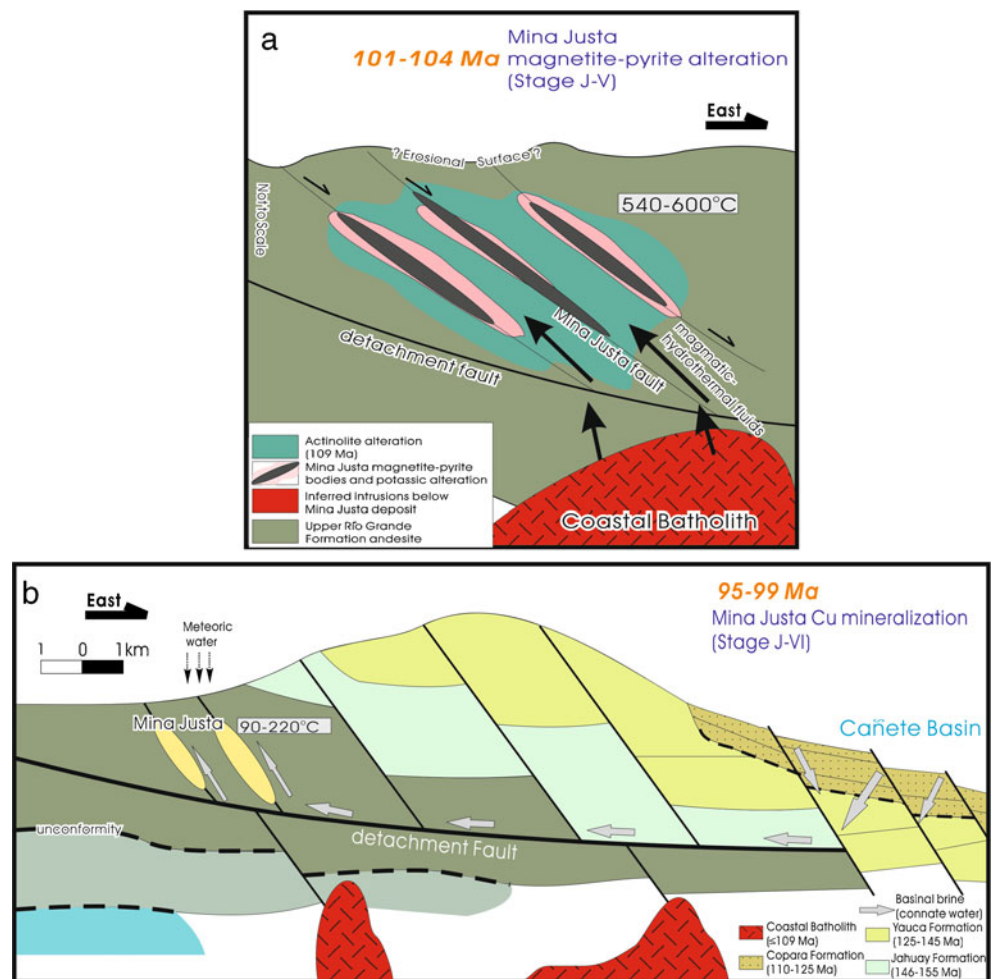


Fig. 15 Cartoon showing the possible evolution of the main magnetite mineralization and major sulphide stage at Marcona (not to scale, age constrained by Chen et al. 2010a)

values (Fig. 11), which show that the dominant fluids are comparable to basinal brines, especially those with high salinities occurring at intermediate latitudes, e.g. California basins (Longstaffe 1987). The $\delta^{34}\text{S}$ values of sulphides from stage J-VI are concentrated in a narrow range around

0‰, but the calculated $\delta^{34}\text{S}_{\text{fluid}}$ values exceed +29‰ (Fig. 13), strong evidence for a non-magmatic source and consistent with data for the main Cu (–Au) ore stages at Raúl-Condastal (Ripley and Ohmoto 1977), La Candelaria (Ullrich and Clark 1999) and Mantoverde (Benavides

Fig. 16 Genetic model for the magnetite–pyrite alteration and Cu mineralization at Mina Justa



et al. 2007). A non-magmatic source for the mineralizing fluid is also supported by the $\delta^{13}\text{C}$ values (Fig. 14), which are similar to those of Marcona late veins (M-VII) and show close analogies to deep formation waters or basinal brines at low latitudes (Fig. 14).

During the Albian, faulting of the Mesozoic volcanic–sedimentary strata along the southwest margin of the Cañete Basin could have provided pathways for fluid circulation (Fig. 16b; Chen et al. 2010a). During tectonic inversion of the basin, Ca-rich basinal brines, possibly derived from connate water in equilibrium with the permeable Copara Formation, would have been expelled from the basin, flowing westward to the Mina Justa area, probably driven by heat from the underlying Coastal Batholith. During their rise to the surface, the basinal fluids replaced early magnetite–pyrite bodies to generate the Cu orebodies, with minor mixing with meteoric waters (Fig. 16b).

Implications for Cu-mineralizing fluids in IOCG deposits

Both the Marcona and Mina Justa deposits share numerous alteration and mineralization characteristics with other major IOCG deposits. Table 8 compares the mineralizing fluids recognized at Mina Justa, Marcona (the hydrothermal polymetallic sulphide stage), major IOCG deposits elsewhere, and several other deposit types which are either iron oxide-rich or potentially affiliated, such as porphyry Cu–Au, stratabound Cu–Ag (mantos) and sediment-hosted Cu deposits.

Recent studies provide strong evidence that high-temperature (>350°C) fluids of at least partial magmatic derivation are responsible for Cu–Au mineralization in some IOCG deposits (Pollard 2001), e.g. Ernest Henry (Mark et al. 2000; Kendrick et al. 2007) and La Candelaria (early polymetallic ore stage and main ore stage: Ullrich and Clark 1999). However, fluid inclusion data from Mina Justa and Marcona indicate that the main sulphide deposition occurred at either low temperatures (<200°C in the case of the Mina Justa Cu mineralization) or over wide temperature range (160–360°C for the Marcona polymetallic sulphide stage), which may imply the involvement of low-temperature external fluids. Similar conditions are documented for the mineralizing stages at the Olympic Dam deposit (~180°C: Oreskes and Einaudi 1992), Lightning Creek (late chalcopyrite veins, 120–180°C: Perring et al. 2000) and Eloise (100–500°C: Baker 1998) in Australia; Mantoverde (150–360°C: Vila et al. 1996) in Chile; Wernecke Breccias (70–350°C: Hunt et al. 2005, 2007) in Canada; Aitik (130–240°C, bornite stage: Wanhainen et al. 2003) in Sweden; and Salobo (173–485°C: Requia et al. 2003) in Brazil. In contrast, porphyry Cu–Au deposits, which are generally magnetite-rich, commonly formed at

consistently high temperatures (300°C to >400°C) for Cu–Au mineralization (Table 8), whereas low-temperature fluids are commonly associated with stratabound Cu–Ag (El Soldado: Boric et al. 2002) and sediment-hosted Cu deposits (Nchanga: McGowan et al. 2006), which may reflect conditions similar to those for IOCG Cu (–Au) mineralization.

High-salinity fluids responsible for Cu–Au mineralization have been documented in many major IOCG deposits (Oreskes and Einaudi 1992; Ullrich and Clark 1999; Pollard 2001; Wanhainen et al. 2003). Whereas most porphyry Cu–Au deposits are products of high-salinity fluids dominated by Na and K, a high content of Ca had been commonly identified in Cu mineralization stage fluids in IOCG deposits (Table 8). These Ca-rich fluids also commonly occur in stratabound Cu–Ag and sediment-hosted Cu deposits in which evaporitic fluids may have contributed to mineralization (Boric et al. 2002; McGowan et al. 2006). Whereas CO_2 has been inferred to play an important role in many IOCG deposits through the unmixing of magmatic $\text{H}_2\text{O}-\text{CO}_2-\text{NaCl} \pm \text{CaCl}_2-\text{KCl}$ fluids (Xu and Pollard 1999; Pollard 2001; Fu et al. 2003), the relationship between this process and Cu (Au–Ag–REE–U) mineralization is not clear. At Ernest Henry, Bidjovagge and, probably, La Candelaria, the high-temperature mineralizing fluids contain considerable CO_2 (Table 8) and are inferred to be responsible for Cu–Au mineralization (Ullrich and Clark 1999; Mark et al. 2000). However, only minor or negligible CO_2 contributed to the Cu mineralization stages at many IOCG deposits, such as Mina Justa, Mantoverde and the Wernecke Breccias (Table 8), which indicates that CO_2 -rich fluids are not a prerequisite for Cu mineralization in IOCG deposits.

Conclusions

The contiguous Middle Jurassic Marcona Fe deposit (156–162 Ma) and Early Cretaceous Mina Justa Cu deposit (95–104 Ma) were generated by different magmatic–hydrothermal systems. At Marcona, the major magnetite orebodies are interpreted as recording an evolution from high-temperature (700–800°C) and hydrous Fe oxide-dominated melts to rapidly cooling (430–600°C) endogenous hydrothermal fluids with dominantly magmatic isotopic compositions. The subsequent lower temperature (160–360°C) polymetallic sulphide stage may record the invasion of seawater modified through reaction with the andesitic host rocks. However, the sulphide vein systems contain only uneconomic Cu, probably recording the restricted mineralization potential of the vesiculating oxide melts (cf. Broman et al. 1999).

Whereas the early magnetite–pyrite assemblage at Mina Justa was deposited from 540°C to 600°C, Na-rich

Table 8 Copper ore-forming fluids involved in IOCG mineralization¹⁾ and other deposit types

| Deposits | Mineral assemblages ^a | Temperature (°C) | Salinity ^b | Dominant cations ^b | Other features | References |
|---|-------------------------------------|----------------------------|-------------------------|-------------------------------|--|--|
| IOCG: Mina Justa, Perú | cp-bn-cc-cal-hm | 85–200 (140) | 6–32 (24) | Ca, Na (–K) | CO ₂ -poor ^c | This study |
| Marcona, Perú | cp-py-po-cal-amph | 70–300 (120 ^d) | 5–33 (20 ^d) | Na, Mg (–Fe), Ca | CO ₂ -poor | This study |
| Raúl, Perú | cp-py-po-qtz±mt | 320–360 (350) | >20 | Na (Ca?) | | Ripley and Ohmoto (1977) |
| Mantoverde, Chile | cp-hm(–cal-qtz) | 150–360 (240) | 14–40 | Na (Ca?) | CO ₂ -poor | Vila et al. 1996 |
| La Candelaria, Chile | cp-po-qtz-amph ± mt | 300–450 | High | Na (Ca) | CO ₂ -rich | Ullrich and Clark (1999) |
| Olympic Dam, Australia | cp-bn-cc-ser- <i>fl</i> -qtz-bar-hm | 130–280 (180) | 7.3–42 | Ca, Na | CO ₂ -bearing | Oreskes and Einaudi (1992) |
| Ernest Henry, Australia | cp-py-mt-cal-qtz-bt-kfs | >350–400 | >26 | Na (Ca?) | CO ₂ -rich | Mark et al. 2000 |
| Eloise, Australia | cp-po-qtz-cal-mt-chl | 100–500 (220) | 30–47 | Ca, Na | CO ₂ -bearing | Baker 1998 |
| Starra, Australia | cp-py-qtz-cal-hm-chl | 220–360 | 29–42 | Ca, Na | CO ₂ -poor | Williams et al. 2001 |
| Osborne, Australia | cp-qtz-cal-chl±mt | ~300 | 20–37 | Na, K, Ca | CO ₂ -bearing | Adshhead et al. 1998 |
| Lightning Creek, Australia | cp-py-cal-chl | 120–180 | 15–28 | Ca, Na | CO ₂ -poor | Perring et al. 2000 |
| Tennant Creek, Australia | cp-py-qtz-chl-hm | 300–340 | 3–10 | Na, Ca | CO ₂ -poor | Skirrow and Walsh 2002 |
| Aitik, Sweden | bn-cc-mt-qtz | 130–220 | 18–27 | Ca, Na | CO ₂ -poor | Wanhainen et al. 2003 |
| Pahtohavare, Sweden | cp-py-po-qtz-cal±mt | 80–350 (120) | 0.5–30 | Ca, Na | CO ₂ -bearing | Lindblom et al. 1996 |
| Bidjovagge, Norway | cp-py-po-qtz-cal±mt | 300–370 | 30–45 | Na, Ca | CO ₂ -CH ₄ -rich | Etmér et al. 1994 |
| Wernecke, Canada | cp-py-qtz-cal±mt±hm | 70–350 (200) | 24–42 | Ca, Na | CO ₂ -poor | Gillen et al. 2004; Hunt et al. 2005, 2007 |
| Salobo, Brazil | cp-bn-cc-qtz-chl | 173–485 | 39–52 | Na (Ca?) | CO ₂ -bearing | Requia et al. 2003; Pollard 2001 |
| <i>Porphyry Cu-Au</i> : Panguna, Papua New Guinea | cp-py-qtz | 350–700 (?) | 46–76 | Na, K | CO ₂ -bearing | Eastoe 1978 |
| Bajo de la Alumbreira, Argentina | cp-py-qtz | 300–400 | 35–65 | Na, K | CO ₂ -bearing | Ulrich et al. 2001 |
| <i>Stratabound Cu-Ag</i> : El Soldado, Chile | cp-bn-cc-cal-hm | 140–180 | 21–34 | Ca, Na | CO ₂ -poor | Boric et al. 2002 |
| Coastal cordillera of northern Chile | cp-bn-cc-cal-qtz-hm | 200–380 (250) | 7–34 | Na, Ca | CO ₂ -poor | Kojima et al. 2003 |
| <i>Sediment-hosted Cu</i> : Nchanga, Zambia | cp-bn-cc-dol-phl | 105–300 (170) | 31–38 | Ca, Na | CO ₂ -bearing | McGowan et al. 2006 |

Copper ore-forming fluids involved in IOCG mineralization, exclusively for Cu (Au, Ag, REE, U) mineralization stages

cp chalcopyrite, py pyrite, po pyrrothite, cal calcite, amph amphibole, bn bornite, cc chalcocite, hm hematite, mt magnetite, qtz quartz, ser sericite, fl fluorite, bar barite, kfs k-feldspar, chl chlorite, phl phlogopite, dol dolomite

^a Italicized mineral used for fluid inclusion study

^b Weight per cent NaCl equiv or weight per cent NaCl+CaCl₂ equiv

^c First-cited cation-dominant

^d The majority

^e Defined in this table: CO₂-rich fluid inclusions containing CO₂≥20%; CO₂-bearing: a few fluid inclusions (<20%) contain CO₂; CO₂-poor: no CO₂ identified in fluid inclusions

hydrothermal fluids with a magmatic signature, the Cu (–Ag) orebodies were entirely the product of low-temperature ($\leq 200^\circ\text{C}$) Ca-rich brines with sulphur and oxygen isotopic compositions predicating a dominant evaporite-sourced basinal brine reservoir. Ore formation is inferred to have taken place during inversion of the contiguous Aptian–Albian Cañete back-arc basin, fluid migration being focused by the intrusion of flanking granitoid plutons of the Coastal Batholith.

For those magnetite-dominant, “Kiruna-type” Fe deposits, such as Kiruna, El Laco and the Cretaceous Chilean iron deposits, a high-temperature, Fe-oxide dominant melt was probably responsible for the massive magnetite mineralization, whereas in probably the majority of Cu-rich IOCG deposits, including Mina Justa, La Candelaria-Punta del Cobre, Mantoverde and Raúl-Condestable, non-magmatic, “exotic” fluids were a prerequisite for economic Cu (–Au, Ag) mineralization.

Acknowledgements This research was supported logistically by Shougang Hierro Perú SA, Chariot Resources and Rio Tinto Mining and Exploration Ltd. which gave permission for this publication, and by National Science and Engineering Research Council of Canada operating grants to Alan H. Clark and T. Kurtis Kyser and equipment grants to the latter. Dr. Louise Corriveau and Dr. Mark Barton are thanked for their comments which have greatly improved this paper. Kerry Klassen provided expert assistance in the stable isotope analysis. LA-TOF-ICPMS analysis was carried out in collaboration with April Vuletic and Rui Zhang at Queen’s University. Discussions with Gregory Lester, Allan Montgomery and Jorge Benavides provided considerable insight.

References

- Adshead ND, Voulgaris P, Muscio VN (1998) Osborne copper–gold deposit. In: Berkman DA, Mackenzie DH (eds) *Geology of Australian and Papua New Guinean mineral deposits*. The Australasian Institute of Mining and Metallurgy, Melbourne, pp 793–799
- Aguirre L (1988) Chemical mobility during low-grade metamorphism of a Jurassic lava flow: Río Grande Formation, Peru. *J S Am Earth Sci* 1:343–361
- Alt JC (1999) Very low-grade hydrothermal metamorphism of basic igneous rocks. In: Frey M, Robinson D (eds) *Low-grade metamorphism*. Blackwell Science, Oxford, pp 169–201
- Atherton MP, Webb S (1989) Volcanic facies, structure, and geochemistry of the marginal basin rocks of central Peru. *J S Am Earth Sci* 2:241–261
- Baker T (1998) Alteration, mineralization, and fluid evolution at the Eloise Cu–Au deposit, Cloncurry District, Northwest Queensland, Australia. *Econ Geol* 93:1213–1236
- Baker T, Perkins C, Blake KL, Williams PJ (2001) Radiogenic and stable isotope constraints on the genesis of the Eloise Cu–Au deposit, Cloncurry district, NW Queensland. *Econ Geol* 96:723–742
- Balcerzak M (2003) An overview of analytical applications of time of flight mass spectrometric (TOF-MS) analysers and an inductively coupled plasma-TOF-MS technique. *Anal Sci* 19:979–989
- Baldassaro PM, Bodnar RJ (2000) Low temperature phase relations in the system $\text{H}_2\text{O}-\text{NaCl}-\text{FeCl}_2$: application to fluid inclusion studies. *Geol Soc Am Abstr Program A-4(2):A-4*
- Barton PB Jr, Skinner BJ (1979) Sulfide mineral stabilities. In: Barnes HL (ed) *Geochemistry of hydrothermal ore deposits*. Wiley, New York, pp 278–403
- Barton MD, Johnson DA (1996) Evaporitic-source model for igneous-related Fe oxide–(REE–Cu–Au–U) mineralization. *Geology* 24:259–262
- Barton MD, Johnson DA (2000) Alternative brine sources for Fe-oxide (–Cu–Au) systems: implications for hydrothermal alteration and metals. In: Porter TM (ed) *Hydrothermal iron oxide copper–gold and related deposits: a global perspective*. Austral Miner Fund, Adelaide, pp 43–60
- Barton MD, Johnson DA (2004) Footprints of Fe-oxide (–Cu–Au) systems. *Univ W Aust Spec Publ* 33:112–116
- Bastrakov EN, Skirrow RG, Davidson GJ (2007) Fluid evolution and origins of iron oxide Cu–Au prospects in the Olympic Dam district, Gawler Craton, South Australia. *Econ Geol* 102:1415–1440
- Baxter R, Meder K, Cinitis R, Berezowski M (2005) The Marcona copper project—Mina Justa prospect geology and mineralisation. *Proceedings of the 3rd Congr Int de Prospectores y Exploradores, Lima, Conferencias, Inst de Ingenieros de Minas del Perú, Lima (CD-ROM)*
- Benavides R, Kyser TK, Clark AH, Oates C, Zamora R, Tamovschi R, Castillo B (2007) The Mantoverde iron oxide–copper–gold district, III Región, Chile: the role of regionally-derived, non-magmatic fluid contributions to chalcopyrite mineralization. *Econ Geol* 102:415–440
- Bodnar R (2003) Introduction to fluid inclusions. In: Samson I, Anderson A, Marshall D (eds) *Fluid inclusion-analysis and interpretation*. Miner Assoc Canada Short Course Series 32, pp 1–9
- Boric R, Holmgren C, Wilson NSF, Zentilli M (2002) The geology of the El Soldado manto type Cu (Ag) deposit, central Chile. In: Porter TM (ed) *Hydrothermal iron oxide–copper–gold & related deposits: a global perspective*. Austral Miner Fund, Adelaide, pp 123–136
- Bottinga Y, Javoy M (1973) Comments on oxygen isotope geothermometry. *Earth Planet Sci Lett* 20:250–265
- Bouzari F, Clark AH (2006) Prograde evolution and geothermal affinities of a major porphyry copper deposit: the Cerro Colorado hypogene protore, I Región, northern Chile. *Econ Geol* 101:95–134
- Bowers TS (1989) Stable isotope signatures of water–rock interaction in mid-ocean ridge hydrothermal systems: sulphur, oxygen, and hydrogen. *J Geophys Res* 94:5775–5786
- Broman C, Nyström JO, Henriquez F, Elfman M (1999) Fluid inclusions in magnetite-apatite ore from a cooling magmatic system at El Laco, Chile. *Geologiska Föreningens i Stockholm Förhandlingar* 121:253–267
- Caldas J (1978) *Geología de los cuadrángulos de San Juan, Acarí y Yauca*. Instituto Geológico Minero y Metalúrgico del Perú, Lima, Perú, Boletín 30
- Chen HY, Clark AH, Kyser TK, Ullrich TD, Baxter R, Chen YM, Moody TC (2010a) Evolution of the giant Marcona–Mina Justa iron oxide–copper–gold district, south-central Peru. *Econ Geol* 105:155–185
- Chen HY, Clark AH, and Kyser TK (2010b) The Marcona magnetite deposit, Ica, central-south Peru: a product of hydrous, iron oxide-rich melt? *Econ Geol* 105:1441–1456
- Clayton RN, Keiffer SW (1991) Oxygen isotopic thermometer calibrations. In: Taylor HP, O’Neil JR, Kaplan IR (eds) *Stable isotope geochemistry: a tribute to Samuel Epstein*. The Geochemical Society Special Publication 3, pp 3–10

- Clayton R, Mayeda TK (1963) The use of bromine pentafluoride in the extraction of oxygen from oxides and silicates for isotopic analysis. *Geochim Cosmochim Acta* 27:43–52
- Clayton RN, O'Neil JR, Mayeda TK (1972) Oxygen isotope exchange between quartz and water. *J Geophys Res* 77:3057–3067
- Davis DW, Lowenstein TK, Spencer RJ (1990) Melting behavior of fluid inclusions in laboratory-grown halite crystals in the systems NaCl–H₂O, NaCl–KCl–H₂O, NaCl–MgCl₂–H₂O, and NaCl–CaCl₂–H₂O. *Geochim Cosmochim Acta* 54:591–601
- de Haller A, Zúñiga AJ, Corfu F, Fontboté L (2002) The iron oxide–Cu–Au deposit of Raúl-Condestable, Mala, Lima, Peru. *Resúmen 11th Congr Geol Peruano*, p 80
- de Haller A, Corfu F, Fontboté L, Schaltegger U, Barra F, Chiaradia M, Frank M, Alvarado JZ (2006) Geology, geochronology, and Hf and Pb isotope data of the Raúl-Condestable iron oxide–copper–gold deposit, central coast of Peru. *Econ Geol* 101:281–310
- Eastoe CJ (1978) A fluid inclusion study of the Panguna porphyry copper deposit, Bougainville, Papua New Guinea. *Econ Geol* 73:721–748
- Ettner DC, Bjolykke A, Andersen T (1994) A fluid inclusion and stable isotope study of the Proterozoic Bidjovagge Au–Cu deposit, Finnmark, northern Norway. *Miner Depos* 29:16–29
- Fisher LA, Kendrick MA (2008) Metamorphic fluid origins in the Osborne Fe oxide–Cu–Au deposit, Australia: evidence from noble gases and halogens. *Miner Depos* 43:483–497
- Fu B, Williams PJ, Oliver NHS, Dong G, Pollard PJ, Mark G (2003) Fluid mixing versus unmixing as an ore-forming process in the Cloncurry Fe-oxide–Cu–Au district, NW Queensland, Australia: evidence from fluid inclusions. *J Geochem Explor* 78(79):617–622
- Gillen D, Baker T, Hunt J, Ryan C, Win TT (2004) PIXE analysis of hydrothermal fluids in the Wernecke Mountains, Canada. *Predictive Mineral Discovery CRC Conference, Barossa Valley, Australia*, pp 69–73
- Goldstein RH (2003) Petrographic analysis of fluid inclusions. In: Samson I, Anderson A, Marshall D (eds) *Fluid inclusion-analysis and interpretation*. Mineralogical Association of Canada Short Course Series 32, pp 9–54
- Goldstein RH, Reynolds TJ (1994) Systematics of fluid inclusions in diagenetic minerals. *Soc Sedim Geol Short Course* 31:199
- Groves DI, Bierlein FP, Meinert LD, Hitzman MW (2010) Iron oxide copper–gold (IOCG) deposits through earth history: implications for origin, lithospheric setting, and distinction from other epigenetic iron oxide deposits. *Econ Geol* 105:641–654
- Harmon RS, Barreiro BA, Moorbath S, Hoefs J, Francis PW, Thorpe RS, Déruelle B, McHugh J, Viglino JA (1984) Regional O-, Sr-, and Pb-isotope relationships in late Cenozoic calc-alkaline lavas of the Andean Cordillera. *J Geol Soc Lond* 141:803–822
- Hawkes N, Clark AH, Moody TC (2002) Marcona and Pampa de Pongo: giant Mesozoic Fe–(Cu, Au) deposits in the Peruvian coastal belt. In: Porter TM (ed) *Hydrothermal iron oxide–copper–gold & related deposits: a global perspective*. Austral Miner Fund, Adelaide, pp 115–130
- Haynes DW, Cross KC, Bills RT, Reed MH (1995) Olympic Dam ore deposit: a fluid-mixing model. *Econ Geol* 90:281–307
- Hedenquist JW, Arribas AJ, Reynolds TJ (1998) Evolution of an intrusion-centered hydrothermal system: far Southeast-Lepanto porphyry and epithermal Cu–Au deposits, Philippines. *Econ Geol* 93:373–404
- Hinton RW (1999) NIST SRM 610, 611 and SRM 612, 613 multi-element glasses: constraints from element abundance ratios measured by microprobe techniques. *Geostand News* 23(2):197–207
- Hoefs J (1997) *Stable isotope geochemistry*, 4th edn. Springer, Berlin, p 214
- Hunt J, Baker T, Thorkelson D (2005) Regional-scale Proterozoic IOCG-mineralized breccia systems: examples from the Wernecke Mountains, Yukon, Canada. *Miner Depos* 40:492–514
- Hunt J, Baker T, Thorkelson D (2007) A review of iron oxide copper–gold deposits, with focus on the Wernecke Breccias, Yukon, Canada, as an example of a non-magmatic end member and implications for IOCG genesis and classification. *Explor Min Geol* 16:209–232
- Javoy M, Pineau F, Cheminee JL, Kraft M (1988) The gas–magma relationship in the 1988 eruption of Oldoinyo Lengai (Tanzania). *Am Geophys Union EOS Trans* 69:1466
- Kajiwra Y, Krouse HR (1971) Sulfur isotope partitioning in metallic sulfide systems. *J Can Earth Sci* 8:1397–1408
- Kendrick MA, Mark G, Phillips D (2007) Mid-crustal fluid mixing in a Proterozoic Fe oxide–Cu–Au deposit, Ernest Henry, Australia: evidence from Ar, Kr, Xe, Cl, Br and I. *Earth Planet Sci Lett* 256:328–343
- Kojima S, Astudillo J, Rojo J, Tristá D, Hayashi K (2003) Ore mineralogy, fluid inclusion, and stable isotopic characteristics of stratiform copper deposits in the coastal Cordillera of northern Chile. *Miner Depos* 38:208–216
- Kyser TK, O'Neil J (1984) Hydrogen isotope systematics of submarine basalts. *Geochim Cosmochim Acta* 48:48–53
- Kyser TK, Leshner CE, Walker D (1998) The effects of liquid immiscibility and thermal diffusion on oxygen isotopes in silicate liquids. *Contrib Mineral Petrol* 133:373–381
- Leach AM, Hieftje GM (2001) Standardless semiquantitative analysis of metals using single-shot laser ablation inductively coupled plasma time-of-flight mass spectrometry. *Anal Chem* 73:2959–2967
- Lindblom S, Broman C, Martinsson O (1996) Magmatic–hydrothermal fluids in the Pahtohavare Cu–Au deposit in greenstone at Kiruna, Sweden. *Miner Depos* 31:307–318
- Longstaffe FJ (1987) Stable isotope studies of diagenetic processes. In: Kyser TK (ed) *Stable isotope geochemistry of low temperature fluids*. Mineralogical Association of Canada Short Course Series 13, pp 187–257
- Mahoney P, Li G, Hieftje GM (1996) Laser ablation–inductively coupled plasma mass spectrometry with a time-of-flight analyzer. *J Anal At Spectrom* 11:401–405
- Mark G, Oliver NHS (2006) Mineralogical and chemical evolution of the Ernest Henry Fe oxide–Cu–Au ore system, Cloncurry district, northwest Queensland, Australia. *Miner Depos* 40:769–801
- Mark G, Oliver NHS, Williams PJ, Valenta RK, Crookes RA (2000) The evolution of the Ernest Henry Fe-oxide–(Cu–Au) hydrothermal system. In: Porter TM (ed) *Hydrothermal iron oxide–copper–gold and related deposits: a global perspective*. Austral Miner Fund, Adelaide, pp 123–136
- Marschik R, Fontboté L (2001) The Candelaria–Punta del Cobre iron oxide Cu–Au (–Zn, Ag) deposits, Chile. *Econ Geol* 96:1799–1826
- McGowan RR, Roberts S, Boyce AJ (2006) Origin of the Nchanga copper–cobalt deposits of the Zambian Copperbelt. *Miner Depos* 40:617–638
- Mukasa SB, Henry DJ (1990) The San Nicolás Batholith of coastal Peru: Early Paleozoic continental arc or continental rift magmatism. *J Geol Soc Lond* 147:27–39
- Naslund HR, Henríquez F, Nyström JO, Vivallo W, Dobbs FM (2002) Magmatic iron ores and associated mineralization: examples from the Chilean High Andes and Coastal Cordillera. In: Porter TM (ed) *Hydrothermal iron oxide–copper–gold & related deposits: a global perspective*. Austral Miner Fund, Adelaide, pp 207–228
- Nielsen H (1979) Sulfur isotopes. In: Jager E, Hunziker J (eds) *Lectures in isotope geology*. Springer, Berlin, pp 283–312

- O'Neil JR, Clayton RN, Mayeda TK (1969) Oxygen isotope fractionation in divalent metal carbonates. *J Chem Phys* 51:5547–5558
- Oakes CS, Bodnar RJ, Simonson JM (1990) The system NaCl–CaCl₂–H₂O: I. The ice liquidus at 1 atm total pressure. *Geochim Cosmochim Acta* 54:603–610
- Ohmoto H, Goldhaber M (1997) Sulphur and carbon isotopes. In: Barnes HL (ed) *Geochemistry of hydrothermal ore deposits*. Wiley, New York, pp 517–611
- Ohmoto H, Rye RO (1979) Isotopes of sulphur and carbon. In: Barnes HL (ed) *Geochemistry of hydrothermal ore deposits*. Wiley, New York, pp 509–567
- Oliveo GR, Chang F, Kyser TK (2006) Formation of the auriferous and barren North Dipper Veins in the Sigma Mine, Val d'Or, Canada: constraints from structural, mineralogical, fluid Inclusion, and isotopic data. *Econ Geol* 101:607–631
- Oreskes N, Einaudi MT (1992) Origin of hydrothermal fluids at Olympic Dam: preliminary results from fluid inclusion and stable isotopes. *Econ Geol* 87:64–90
- Perring CS, Pollard PJ, Dong G, Nunn AJ, Blake KL (2000) The Lightning Creek sill complex, Cloncurry district, Northwestern Queensland: a source of fluids for the Fe oxide Cu–Au mineralization and sodic–calcic alteration. *Econ Geol* 95:1037–1089
- Pollard PJ (2000) Evidence of a magmatic fluid and metal source for Fe-oxide Cu–Au mineralization. In: Porter TM (ed) *Hydrothermal iron oxide–copper–gold and related deposits: a global perspective*. Austral Miner Fund, Adelaide, pp 27–41
- Pollard PJ (2001) Sodic(–calcic) alteration associated with Fe-oxide–Cu–Au deposits: An origin via unmixing of magmatic-derived H₂O–CO₂–salt fluids. *Miner Depos* 36:93–100
- Pollard PJ (2006) An intrusion-related origin for Cu–Au mineralization in iron oxide–copper–gold (IOCG) provinces. *Miner Depos* 41:179–187
- Requia K, Stein H, Fontboté L, Chiaradia M (2003) Re–Os and Pb–Pb geochronology of the Archean Salobo iron oxide copper–gold deposit, Carajás mineral province, northern Brazil. *Miner Depos* 38:727–738
- Rhodes AL, Oreskes N, Sheets S (1999) Geology and rare earth element geochemistry of magnetic deposits at El Laco, Chile. *Soc Econ Geol Spec Publ* 7:299–332
- Ripley EM, Ohmoto H (1977) Mineralogical, sulphur isotope, and fluid inclusion studies of the stratabound copper deposits at the Raúl mine, Peru. *Econ Geol* 72:1017–1041
- Roedder E (1984) Fluid inclusions. *Mineralogical Society of America Rev Miner* 12:646
- Rotherham JF, Blake KL, Cartwright I, Williams PJ (1998) Stable isotope evidence for the origin of the Mesoproterozoic Starra Au–Cu deposit, Cloncurry district, northwest Queensland. *Econ Geol* 93:1435–1449
- Seedorff E, Einaudi M (2004) Henderson porphyry molybdenum system, Colorado: II. Decoupling of introduction and deposition of metals during geochemical evolution of hydrothermal fluids. *Econ Geol* 99:39–72
- Sharma T, Clayton RN (1965) Measurement of ¹⁸O/¹⁶O ratios of total oxygen of carbonates. *Geochim Cosmochim Acta* 29:1347–1353
- Sillitoe RH, Burrows DR (2002) New field evidence bearing on the origin of the El Laco magnetite deposit, northern Chile. *Econ Geol* 97:1101–1109
- Skirrow RG, Walsh JL (2002) Reduced and oxidized Au–Cu–Bi deposits of the Tennant Creek inlier, Australia: an integrated geologic and chemical model. *Econ Geol* 97:1167–1202
- Smith MP, Henderson P (2000) Preliminary fluid inclusion constraints on fluid evolution in the Bayan Obo Fe–REE–Nb deposit, Inner Mongolia, China. *Econ Geol* 95:1371–1388
- Suzuoki T, Epstein S (1976) Hydrogen isotope fractionation between OH-bearing minerals and water. *Geochim Cosmochim Acta* 40:1229–1240
- Syn Flint Inc. (1985) *Synthetic fluid inclusions: manual accompanying synthetic fluid inclusions*. State College, Pennsylvania, p 34
- Taylor BE (1986) Magmatic volatiles: isotopic variation of C, H and S. *Rev Miner* 16:185–271
- Taylor HP (1997) Oxygen and hydrogen isotope relationships in hydrothermal mineral deposits. In: Barnes HL (ed) *Geochemistry of hydrothermal ore deposits*. Wiley, New York, pp 229–302
- Taylor HP, Epstein S (1962) Relationship between ¹⁸O/¹⁶O ratios in coexisting minerals of igneous and metamorphic rocks, part I. *Geol Soc Am Bull* 73:461–480
- Ullrich TD, Clark AH (1999) The Candelaria Cu–Au deposit, III Región, Chile: paragenesis, geochronology and fluid composition. In: Stanley CJ et al (eds) *Mineral deposits: processes to processing*. Balkema, Rotterdam, pp 201–204
- Ullrich TD, Clark AH, Kyser TK (2001) The Candelaria Cu–Au deposit, III Región, Chile: product of long-term mixing of magmatic-hydrothermal and evaporite-sourced fluids. *GSA Annual Meeting, Boston, Abstracts with Programs*, p A-3
- Ulrich T, Guenther D, Heinrich CA (2001) The evolution of a porphyry Cu–Au deposit, based on LA-ICP-MS analysis of fluid inclusions; Bajo de la Alumbrera, Argentina. *Econ Geol* 96:1743–1774
- Valley JW (2003) Oxygen isotopes in zircon. In: Hanchar JM, Hoskin PWO (eds) *Zircon*. *Rev Mineral Geochem* 53:343–385
- Vidal CE, Injoque-Espinoza JL, Sidder GB, Mukasa SB (1990) Amphibolitic Cu–Fe skarn deposits in the central coast of Peru. *Econ Geol* 85:1447–1461
- Vila T, Lindsay N, Zamora R (1996) Geology of the Mantoverde copper deposit, northern Chile: a specularite-rich, hydrothermal–tectonic breccia related to the Atacama Fault Zone. In: Camus F, Sillitoe RH, Petersen R (eds) *Andean copper deposits: new discoveries, mineralization styles and metallogeny*. Society of Economic Geologists, Special Publication 5, pp 157–169
- Wanhainen C, Broman C, Martinsson O (2003) The Aitik Cu–Au–Ag deposit in northern Sweden: a product of high salinity fluids. *Miner Depos* 38:715–726
- Williams PJ (2010) Classifying IOCG deposits. In: *Exploring for iron oxide copper–gold deposits: Canada and global analogues*. Geological Association of Canada, Short Course Notes 20, pp 11–19
- Williams PJ, Dong G, Ryan CG, Pollard PJ, Rotherham JF, Mernagh TP, Chapman LH (2001) Geochemistry of hypersaline fluid inclusions from the Starra (Fe oxide)–Au–Cu deposit, Cloncurry district, Queensland. *Econ Geol* 96:875–883
- Williams PJ, Barton MD, Johnson DA, Fontboté L, Halter AD, Mark G, Oliver NHS, Marschik R (2005) Iron-oxide copper–gold deposits: geology, space-time distribution, and possible modes of origin. *Economic Geology 100th Anniversary Volume*, pp 371–405
- Xu G, Pollard PJ (1999) Origin of CO₂-rich fluid inclusions in synorogenic veins from the Eastern Mount Isa Fold Belt, NW Queensland, and their implications for mineralization. *Miner Depos* 34:395–404
- Zhao ZF, Zheng YF (2003) Calculation of oxygen isotope fractionation in magmatic rocks. *Chem Geol* 193:59–80
- Zheng YF (1993) Calculation of oxygen isotope fractionation in hydroxyl-bearing silicates. *Earth Planet Sci Lett* 120:247–263